Model of Early Diagenesis in the Upper Sediment with Adaptable complexity – MEDUSA (v. 2): a time-dependent biogeochemical sediment module for Earth System Models, process analysis and teaching

Guy Munhoven

Dépt. d'Astrophysique, Géophysique et Océanographie, Université de Liège, B–4000 Liège, Belgium
Correspondence: Guy Munhoven
(Guy.Munhoven@uliege.be)

Abstract. MEDUSA is a time-dependent one-dimensional numerical model of coupled early diagenetic processes in the surface seafloor sediment. In the vertical, the sediment is subdivided into two different zones. Solids (biogenic, mineral, etc.) raining down from the surface of the ocean are collected by the reactive mixed layer at the top. This is where chemical reactions take place. Solids are transported by bioturbation and advection, solutes by diffusion and bioirrigation. The classical coupled

5   time-dependent early diagenesis equations (advection-diffusion reaction equations) are used to describe the evolutions of the solid and solute components here. Solids that get transported deeper than the bottom boundary of the reactive mixed layer enter the second zone underneath, where reactions and mixing are neglected. Gradually as solid material gets transferred here from the overlying reactive layer, it is buried and preserved in a stack of layers that make up a synthetic sediment core.

MEDUSA has been extensively modified since its first release from 2007. The composition of the two phases, the processes

10 (chemical reactions) and chemical equilibria between solutes are not fixed any more, but get assembled from a set of XML based description files that are processed by a code generator to produce the required Fortran code. 1D, 2D and 2D×2D interfaces have been introduced to facilitate the coupling to common grid configurations and material compositions used in biogeochemical models. MEDUSA can also be run in parallel computing environments using the Message Passing Interface (MPI).

15 # 1   Introduction

1.1   Ocean-atmosphere exchange schemes: an overview

Ocean biogeochemical cycle models call upon a variety of schemes of different complexity levels to represent ocean-sediment exchange fluxes. These can be classified into four major categories (Hülse et al., 2017): (1) reflective boundary conditions; (2) semi-reflective or conservative; (3) vertically-integrated dynamic models; (4) vertically resolved diagenetic models. These

20 categories are similar but not identical to the levels in the classification of Soetaert et al. (2000): categories 3 and 4 respectively correspond to their level 3 and 4 descriptions; category 1 fits their level 2 description, while category 2 generalises this latter.

Reflective boundary conditions are the simplest of these: material reaching the model sea-floor (i.e., the deepest layer in the model water column) is unconditionally remineralised (oxidized, dissolved) there. Global mass conservation is obviously guaranteed with this approach, but the approach may be unrealistic in some places: calcite gets dissolved even if the sea-floor

25 bathes in waters that are strongly supersaturated with respect to calcite or organic matter oxidized even if oxygen levels are low. This unrealistic behaviour can to some extent be alleviated with the semi-reflective or conservative scheme. Here, only part of the remineralisation products (nutrients, dissolved inorganic carbon, silica, etc.) of the solids reaching the sea-floor are returned to the bottom water; the remainder is returned to the surface, mimicking riverine input, and once again allowing for global mass conservation. The fraction remineralised can be made to vary in space and time and can also be different

30 for different materials. Carbonate fractions remineralised can, e.g., be linked to the degree of saturation with respect to one carbonate mineral or another, and organic carbon fractions remineralised to the degree of oxygenation of the bottom waters. Both schemes are attractive because of their convenient computational efficiencies. They do, however, not allow to take into account the complexities of the actual remineralisation pathways of the various biogenic components in the surface sediments, nor can they represent the temporary storage of such material in the surface sediment and delayed return of nutrients, dissolved

35 inorganic carbon or silica to the ocean bottom waters.

The vertically-integrated dynamic category 3 encompasses ocean-sediment exchange schemes that explicitly include a single-box representation of the surface sediment. Mass balances of some, if not all, constituents of this single-layer sediment can be traced. Although termed "vertically-integrated" not all of the schemes that fall into this category can be traced back to some actual vertically resolved model that was vertically integrated.

40 Vertically resolved diagenetic models finally represent the most mechanistically oriented alternative to represent ocean-sediment exchange fluxes. Such models can take into account the complex interplay between various diagenetic processes (organic matter remineralisation, mineral dissolution or precipitation) and transport pathways (advection, bioturbation, solute diffusion in porewater, bioirrigation, etc.). They solve a set of coupled standard early diagenesis equations (Boudreau, 1997) for solid and dissolved component concentrations, generally in combination with law of mass action equations for chemical

45 equilibria (e.g., for the carbonate system).

Meta-model approaches, i.e., parametric representations or emulators of comprehensive models, may either fit into the second or the third categories, depending on their design. Such emulators generally come as empirical parametric functions either derived by fitting selected model outcomes (such as diffusive return fluxes) from large sets of simulation experiments carried out with varying boundary conditions to some expert-chosen empirical parametric functions or by analysing complex

50 models with approaches based upon system identification theory.

The actually required complexity of an adopted ocean-sediment exchange scheme depends of course on the application made. For short-term experiments (say a few decades to a few centuries) with high-resolution biogeochemical models carefully calibrated semi-reflective/conservative schemes are generally the only viable, but nevertheless perfectly acceptable option. For long-term applications (simulation experiments exceeding several thousands of years, i.e., several ocean mixing cycles),

55 vertically integrated or resolved schemes are required for realistic model responses to changing boundary conditions and forcings.

Model and Reference	Resolution	Thickness	Core layers
Archer (1991)	10 layers	10 cm	—
Archer (1996a)	13 layers	10 cm	—
HAMOCC 2S (Heinze et al., 1999)	10 layers	10 cm	1
HAMOCC 5.1 (Maier-Reimer et al., 2005)	12 layers	14 cm	1
HAMOCC 5.2 (Ilyina et al., 2013a)	12 layers	14 cm	1
MUDS (Archer et al., 2002)	17 layers	100 cm	—
MEDUSA (v. 1, Munhoven, 2007)	21 nodes	10 cm	n
CESM-MEDUSA (Kurahashi-Nakamura et al., 2020)	21 nodes	10 cm	n
SEDGEM (Ridgwell and Hargreaves, 2007)	$1 + n$ layers	$5 + n$ cm	(included)
DCESS-ESM (Shaffer et al., 2008)	7 layers	10 cm	?
GEOCLIM *reloaded* (Arndt et al., 2011)	∼100 nodes	100 cm	—
C.CANDI (Luff et al., 2000)	1000 layers	25 cm	—
BRNS-global (Jourabchi et al., 2005)	251 nodes	165 cm	—

Table 1. General characteristics of vertically resolved sediment models used in global biogeochemical models and, for comparison, of two high-complexity models (C.CANDI and BRNS-global). n layers means that the number of layers is not fixed but grows as simulations proceed. For GEOCLIM *reloaded*, the number of layers was estimated from the given thicknesses of the top- and the bottom-most layers and the reported grid-point distribution function.

The surface sedimentary mixed-layer, where most of the processing of the deposited biogeochemically relevant material takes place only extends down to about 5 to 15 cm on global average (9.8 ± 4.5 cm according to Boudreau (1994)). As a result of the diagenetic processes in action there, strong concentration gradients are generated and sustained: the amplitude of the concentration differences observed over this depth interval may be comparable to those observed in the more than four orders of magnitude thicker overlying water column (3750 m on average) – see, e.g., the oxygen and pH profile data in section 3.3 below. A realistic explicit representation of the surface sedimentary environment thus requires a vertical resolution of the same order of magnitude in terms of vertical layers or grid points than the complete water column above it. Typical vertically resolved early diagenesis present vertical resolutions of the order of ten to twenty layers (see Tab. 1). For comparison the water column in GENIE-1, which includes SEDGEM, (Ridgwell, 2007; Ridgwell and Hargreaves, 2007) has eight vertical layers, HAMOCC-2S (Heinze et al., 2009) has ten and the more recent HAMOCC 5.2 (Ilyina et al., 2013a) has forty layers.

Accordingly, sea-floor sediment modules (category 3 and 4 schemes) are not yet commonplace in global ocean biogeochemical models. Only four out of fifteen Earth System Models of Intermediate Complexity (EMICs) participating in the EMIC AR5 Intercomparison Project (Eby et al., 2013) are reported to have a sediment module included: Bern3D (Tschumi et al., 2011), DCESS-ESM (Shaffer et al., 2008), GENIE (Ridgwell and Hargreaves, 2007) and UVic 2.9 (Eby et al., 2009); one further participating EMIC, CLIMBER 2, is also routinely used with a sedimentary module included (e.g., Brovkin et al., 2012). Advanced

high-resolution models generally call upon category 1 or 2 schemes for their sea-floor boundary condition, although there are exceptions. The HAMOCC (HAmburg Model of the Oceanic Carbon Cycle) family of models, whose origins reach back to Maier-Reimer (1984), actually has a long-standing history of explicitly taking sedimentary processes into account. HAMOCC 2

75 (Heinze et al., 1991) was the first one to get a fully coupled sediment module (Archer and Maier-Reimer, 1994), the oxic-only version of the calcite dissolution model of Archer (1991). Later, it received a purposely developed sediment module (Heinze et al., 1999; Heinze and Maier-Reimer, 1999). Archer et al. (2000) use HAMOCC 2 coupled to the much more complete diagenetic model MUDS (Archer et al., 2002), which considers the sequence of oxic, suboxic (via NO_3^-, FeOOH and MnO_2 reduction) and anoxic (via SO_4^{2-} reduction) organic matter remineralisation pathways. Later developments of HAMOCC also

80 included suboxic remineralisation pathways of organic matter in the standard sediment model of HAMOCC: in HAMOCC 5.1 (Maier-Reimer et al., 2005) denitrification was added, in HAMOCC 5.2 (Ilyina et al., 2013b) sulfate reduction. Gehlen et al. (2006) have coupled a slightly extended version of the sediment model of Heinze et al. (1999) to PISCES, the biogeochemical component of NEMO, with nitrate reduction and denitrification as an additional remineralisation pathway for organic matter. The Gehlen et al. (2006) model was later also introduced as the sediment component into Bern3D (Tschumi et al., 2011).

85 Box models and box-diffusion models of the ocean carbon cycle have an even longer-standing history of including ocean-sediment schemes. Especially box models have been for a long time the only types of models that could be used to carry out analyses on time scales of several thousands to tens or hundreds of thousands of years. Hoffert et al. (1981) outline the fundamentals of a simple ocean-sediment exchange scheme for their box-diffusion carbon cycle model, but without actually using it in the end and so Keir and Berger (1983) appear to have been the first to couple a vertically-integrated sediment

90 model to a two-box representation of the ocean-atmosphere carbon cycle for their study of glacial-interglacial CO_2 variations. The theoretical foundations of that scheme had been presented in Keir (1982) (see also Munhoven (1997) for a variant and additional details). In that scheme, the surface sediment was assumed to be well-mixed solid phase, with clay and calcite as the only solid components, and with CO_3^{2-} as the only modelled solute in the porewater. Adopting furthermore a calcite dissolution rate proportional to $f(1-\Omega)^n$, where f was the calcite fraction in the solid phase, Ω the degree of supersaturation with respect

95 to calcite and n the dissolution rate order, the steady-state porewater profile of CO_3^{2-} can be calculated. The total dissolution rate can then be set equal to the diffusive flux of CO_3^{2-} at the sediment-water interface (SWI), which is proportional to $\sqrt{f}(1-\Omega_{SWI})^{\frac{n+1}{2}}$. This same scheme and variants of it have afterwards been used in a large variety of box and box-diffusion models, with increasingly better geographical resolution as time evolved: Sundquist (1986), with unreported n, CYCLOPS (Keir, 1988) with $n = 4.5$, Walker and Opdyke (1995) with $n = 1$, MBM (Munhoven and François, 1996; Munhoven, 1997)

100 with $n = 4.5$. Sigman et al. (1998) reconsidered the CYCLOPS model of Keir (1988) and replaced the purely CO_3^{2-} driven dissolution scheme by a meta-model based upon a multivariate polynomial expression fitted to the calcite dissolution rates obtained with the model of Martin and Sayles (1996) under various boundary conditions, also capable of taking the effect of porewater CO_2 derived from the respiration of organic matter on promoting calcite dissolution in the sedimentary mixed-layer. Munhoven (2007) finally replaced the 304 vertically-integrated sediment boxes in MBM by as many vertically resolved and

105 fully coupled MEDUSA-v1 sediment columns (see section 1.2 below for details). The ocean-sediment exchange schemes in all

of the three MBM versions furthermore tracked the history of deposition of the sediment solids and could thus consistently take into account the effect of chemical erosion events.

There are various means to alleviate the computational overburden caused by adding a vertically resolved early diagenesis model to a biogeochemical ocean model. First of all, the number of vertical layers and of chemical constituents or the

110 complexity of the remineralisation reaction network can be reduced. Most EMICs that include a vertically resolved sediment module appear to follow that pathway (see Tables 1 and 2): UVic 2.9 (Eby et al., 2009) and CLIMBER 2 (Brovkin et al., 2012) both include the oxic-only model of Archer (1996a), with thirteen vertical layers; DCESS-ESM (Shaffer et al., 2008) includes a hybrid category 3/4 ocean-sediment exchange scheme considering CO_3^{-2}, O_2 and organic carbon distributions in seven layers, and calcite and clay contents vertically integrated. One may also reduce the number of spatially distributed sediment columns.

115 This approach was adopted for GEOCLIM *reloaded* (Arndt et al., 2011). The ocean module of GEOCLIM *reloaded* consists of an advective-diffusive inner ocean, completed by two two-box (surface and deep) ensembles for the polar and epicontinental seas. The inner ocean is divided into of several hundreds of 10 m thick layers. The ocean-sediment exchange scheme, however, consists of only three vertically resolved sediment columns, attached to the polar, the inner and the epicontinental water-columns, respectively. In each of the three sediment columns the complete cascade of organic matter oxidation pathways from aerobic

120 respiration to NO_3^-, Mn(IV), Fe(III) and SO_4^{2-} reduction to CH_4 formation as well as a series of secondary redox reactions are taken into account. Even with these strongly reduced resolution of the ocean-sediment exchange scheme, the computation impact remains considerable: Arndt et al. (2011) report that one day of CPU allowed for a 1 Myr simulation without sediments, but only for a 100 kyr simulation with sediments. Finally, the ocean-sediment exchange scheme and the ocean biogeochemical calculations may be carried out with different time steps (asynchronous coupling). This approach is followed in GENIE

125 (Ridgwell, 2007; Ridgwell and Hargreaves, 2007) and MBM (Munhoven and François, 1996; Munhoven, 1997, 2007).

Sea-floor sediments are not only relevant as processing "units" for biogenic material raining down from the surface euphotic layer, during which some part gets remineralised (i.e., oxidised or dissolved), and some parts gets buried. Burial is, however, at first only temporary. Changes in the overlying boundary conditions (e.g., saturation conditions) may indeed lead to chemical erosion episodes where the surface sedimentary mixed-layer loses material faster than it is replenished by deposition from the

130 water-column above. We are currently at the onset of such an episode: as ocean acidification due to the uptake of anthropogenic CO_2 progresses to the deep-ocean, the resulting change in the degree of saturation with respect to carbonate minerals is expected to enhance the dissolution of carbonates in the sea-floor surface sediments at depth so strongly that the dissolution rate will exceed the rate at which carbonate material gets deposited at the sediment water interface. Previously buried carbonates will then return to the sedimentary mixed as a result of the bioturbation activity, which tends to keep the surface mixed layer

135 at a rather stable thickness, which seems to be controlled by the supply of organic matter (Boudreau, 1998). Archer (1996b) estimates that existing carbonates in surface sea-floor sediment can neutralize about 1600 GtC, considerably more than the ∼1000 GtC that may at most be emitted while still limiting global anthropogenic temperature change below 2 °C (e.g., Zickfeld et al., 2016), but much less than the estimated resources of fossil fuels of 8,543 – 13,649 GtC (Bruckner et al., 2014, Tab. 7.2).

Finally it should not be forgotten that sea-floor sediments represent our most comprehensive source of information about

140 past climate change and it is of course indispensable to understand how early diagenetic processes influence the sedimentary

Model	Solutes	Solids
Archer (1991)	CO_2, HCO_3^-, CO_3^{2-}, O_2	Clay, Calcite, OrgC
Archer (1996a)	CO_2, HCO_3^-, CO_3^{2-}, $B(OH)_3$, $B(OH)_4^-$, O_2	Clay, Calcite, OrgC
HAMOCC2S (Heinze et al., 1999)	TCO_2, TAlk, O_2, PO_4^{3-}, $Si(OH)_4$	Clay, ^{12}C-Calcite, ^{13}C-Calcite, ^{14}C-Calcite, $Org^{12}C$, $Org^{13}C$, $Org^{14}C$, Opal
HAMOCC5.1 (Maier-Reimer et al., 2005)	TCO_2, TAlk, O_2, PO_4^{3-}, $Si(OH)_4$	Clay, Calcite, OrgC, Opal
HAMOCC5.2 (Ilyina et al., 2013a)	TCO_2, TAlk, O_2, PO_4^{3-}, Si, NO_3^-, Fe, N_2	Clay, Calcite, OrgC, Opal
MUDS (Archer et al., 2000, 2002)	CO_3^{2-}, O_2, NO_3^-, $Si(OH)_4$, Mn^{2+}, Fe^{2+}, NH_4^+	Clay, Calcite, $OrgC_{fast}$, $OrgC_{slow}$, Opal, MnO_2, FeOOH
MEDUSA (v. 1, Munhoven, 2007)	CO_2, HCO_3^-, CO_3^{2-}, O_2	Clay, Calcite, Aragonite, OrgC
CESM-MEDUSA (Kurahashi-Nakamura et al., 2020)	CO_2, HCO_3^-, CO_3^{2-}, O_2 H_4SiO_4, NO_3^-, $DI^{13}C$, $DI^{14}C$	Clay, Calcite, ^{13}C-Calcite, ^{14}C-Calcite, OrgC, $Org^{13}C$, $Org^{14}C$, Opal
SEDGEM (Ridgwell and Hargreaves, 2007)	—	Clay, Calcite, ^{13}C-Calcite, ^{14}C-Calcite,
SEDGEM (Ridgwell, 2007)	—	Clay, Calcite, ^{13}C-Calcite, ^{14}C-Calcite, Opal
DCESS-ESM (Shaffer et al., 2008)	CO_3^{2-}, O_2	(Calcite, Clay,)[a] OrgC
GEOCLIM *reloaded*[b] (Arndt et al., 2011)	TCO_2, TAlk, THS, TB, O_2, PO_4^{3-}, NO_3^-, NH_4^+, Ca^{2+}, SO_4^{2-}, CH_4	POC, PIC
C.CANDI[b] (Luff et al., 2000; Luff and Moll, 2004)	O_2, NO_3^-, Mn^{2+}, Fe^{2+}, SO_4^{2-}, CH_4, TPO_4, TNH_4, H_2S, HS^-, CO_2, HCO_3^-, CO_3^{2-}	MnO_2, $Fe(OH)_3$, $POC_{\#0}$, $POC_{\#1}$, $POC_{\#2}$, FeS
BRNS-global[b] (Jourabchi et al., 2005)	CO_2, HCO_3^-, CO_3^{2-}, O_2, NO_3^-, Mn^{2+}, Fe^{2+}, NH_4^+, Ca^{2+}, SO_4^{2-}, H_2S, HS^-, CH_4, $B(OH)_3$, $B(OH)_4^-$	OrgC, Calcite, MnO_2, $Fe(OH)_3$, FeS, $FeCO_3$, $MnCO_3$

[a] supposed to be well mixed, i. e., only total contents of the bioturbated layer traced.

[b] solids' advection rate profile prescribed and therefore no clay or other inert solid component considered

Table 2. Porewater and solid phase species in sediment models used in global biogeochemical models and, for comparison, in two typical applications of high-complexity models (C.CANDI, which has been coupled to a regional ocean model for short-term applications of a few years only, and BRNS-global, which has been mainly used for steady-state studies of individual stations).

record, and it would be desirable to directly compare generated model (synthetic) sedimentary records to the observed records instead of thus opening new possibilities in terms of data assimilation.

1.2 MEDUSA: from version 1 to version 2

The first version of the Model of Early Diagenesis in the Upper Sediment,[1] MEDUSA – hereafter MEDUSA-v1 – was described

145 in Munhoven (2007). It is a time-dependent vertically resolved biogeochemical model of the early diagenesis processes in the seafloor sediment. MEDUSA-v1 included clay, calcite, aragonite and organic matter as solid components, and CO_2, HCO_3^-, CO_3^{2-} and O_2 as porewater solutes. Besides that configuration, two others (unpublished) had been developed: one which furthermore included opal and dissolved silica and one which also included the ^{13}C isotopic signatures of all carbon-bearing components.

150 Right from the beginning, MEDUSA had been developed as a sediment module for the diverse ocean biogeochemical models used in our research group, ranging from box to three-dimensional models, the latter with diverse grid configurations and also various sets of chemical tracers. Furthermore, our research interests required a model that could be used in studies dealing with time scales ranging from tens of years to hundreds of thousands of years. Accordingly, the model requirements were laid out as follows: (1) the model code should be customizable to accommodate different chemical compositions; (2) the model should

155 offer the possibility to be coupled to strongly different host model grid layouts; (3) it should be possible to run the model with variable time-steps; (4) the model must be able to cope with chemical erosion, i.e., be able to recover previously buried material from deeper layers and to return it to the chemically reactive mixed-layer.

The customization options offered by MEDUSA-v1 had to be selected with pre-processor directives in the code. Extending the capabilities of the model on the basis of that mechanism had become more and more cumbersome and difficult to manage

160 with time. The code was therefore revised in depth and only the parts related to the transport terms in the equations and the equation system solver—the framework system—were kept. The rest of the code was from now on built on purpose for each application with a code configuration and generation tool that would produce and assemble the parts related to the components, processes (reactions) and chemical equilibria required. A code generator was developed to read in the required information, such as chemical and physical properties of components, chemical reactions describing diagenetic processes and chemical

165 equilibria from a series of description files. These description files use a format based upon the eXtensible Markup Language (XML) syntax (W3C, 2008). Organising the information in an XML tree offers attractive flexibility: such a tree can be easily extended for later developments and it is possible to access any particular information wherever it is located in a file. XML thus offers a high degree of compatibility between subsequent versions of the configurator, which can always extract the relevant information as long as the required mark-up tags remain present. Above all, XML files remain mostly human-readable and the

170 possibility to insert comments makes it possible to ensure the traceability of the stored information.

As the complete tool was meant to require only a Fortran compiler to be built, a simple library, called μXML, for reading and processing basic ASCII encoded XML files in Fortran 95 was developed as a prerequisite.

---

[1]The final 'A' did not have any particular meaning initially, although music lovers amongst early diagenetic modellers will undoubtedly have read it as "A♭ minor."
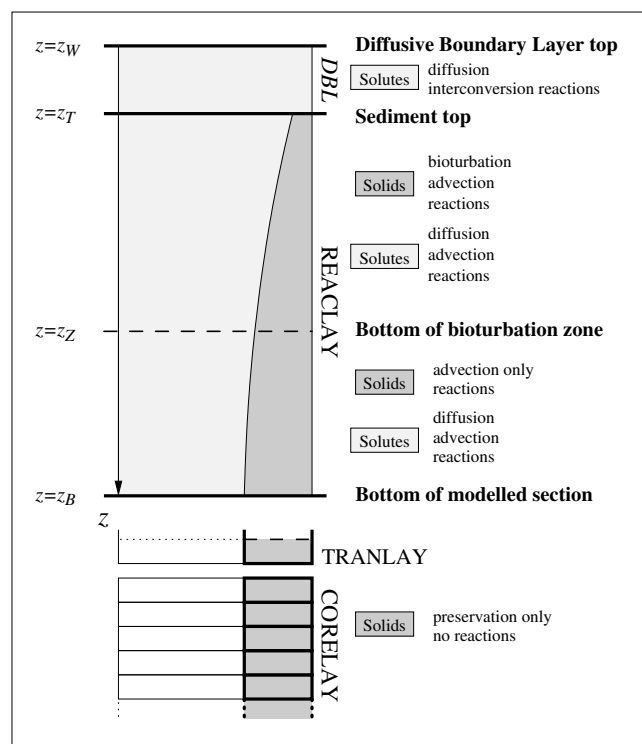
Figure 1. Partitioning of the sediment column in MEDUSA: an optional diffusive boundary layer (DBL) on top of the main part of the model sediment where diagenetic reactions and advective-diffusive transport take place (REACLAY), the transition layer (TRANLAY) and the core represented by the stack of layers (CORELAY). The bottom of the bioturbation zone may coincide with the bottom of REACLAY. If the optional DBL is omitted, $z_W = z_T$. See text for further details.

2 Model Description

2.1 Vertical partitioning of the sediment column

175   The complete sediment column is subdivided into three (or four) different vertically stacked parts (called realms), as illustrated on Fig. 1: (1) REACLAY, the top-most part extending downwards from the sediment top at the sediment-water interface and where the chemical reactions are taken into consideration; (2) TRANLAY, the transition layer of changing thickness just underneath, acting as a temporary storage to connect REACLAY to the underlying (3) CORELAY, a stack of sedimentary layers representing the deep sediment, i. e., the sediment core. Additionally an optional diffusive boundary layer (DBL—not to scale on Fig. 1) acting as a diffusive barrier to the sediment-water exchange of solutes can be included on top of the REACLAY realm.
180   REACLAY includes the bioturbated sedimentary mixed-layer, where most of the reactions relevant for early diagenesis take place (organic matter remineralisation, carbonate dissolution etc.).

2.1.1 Equations in the DBL and REACLAY realms

In the REACLAY realm, MEDUSA solves the standard time-dependent diagenetic equation (e.g., Berner, 1980; Boudreau, 1997),
185 which can be written for each sediment component i (solid or solute) in generic form as

$$\frac{\partial \hat{C}_i}{\partial t} + \frac{\partial \hat{J}_i}{\partial z} - \hat{S}_i = 0. \tag{1}$$

In this equation, t is time and z depth below the sediment-water interface (positive downwards – see Fig. 1). $\hat{C}_i$ denotes the concentration of i in moles for solutes and in kg for solids per unit volume of total sediment (solids plus porewater). $\hat{J}_i$ is the local transport (advection and diffusion), per unit surface area of total sediment. $\hat{S}_i = \hat{R}_i + \hat{r}_i + \hat{Q}_i$ represents the net
190 source-minus-sink balance for constituent i per unit volume of total sediment, where $\hat{R}_i$ is the net reaction rate, equal to the difference between production and destruction (or decay) rates, $\hat{r}_i$ is the net fast reaction rate, that is going to be filtered out of the equations by equilibrium considerations and $\hat{Q}_i$ the non-local transport (considered only for solutes). The total sediment concentrations $\hat{C}_i$ are related to the more directly accessible phase-specific concentrations C_i^{s} (for solids) and C_i^{f} (for solutes) by $\hat{C}_i = \varphi^{\mathrm{s}} C_i^{\mathrm{s}}$ and $\hat{C}_i = \varphi^{\mathrm{f}} C_i^{\mathrm{f}}$, respectively. φ^{s} and φ^{f} denote the volume fraction of bulk solids and of porewater in the total
195 sediment, linked to porosity φ by $\varphi^{\mathrm{s}}(z) = 1 - \varphi(z)$ and $\varphi^{\mathrm{f}}(z) = \varphi(z)$. The porosity profile $\varphi(z)$ is prescribed but may be different for each column in multi-column set-ups.

In the DBL (if any), only equations for solutes are considered and porosity is set to 1. Solids are supposed to rain through the DBL and directly enter REACLAY at its top surface.

Transport

200 Solids are transported by advection throughout the sediment column and subject to bioturbation in the surface mixed layer. Bioturbation is represented as a diffusive process. Both inter- and intraphase biodiffusion variants (Boudreau, 1986) are taken into account and can be combined. With interphase biodiffusion the bulk sediment gets mixed by infaunal activity, solids and porewater alike, and porosity gradients are thus affected as well; with intraphase biodiffusion only the solid phase constituents get mixed:

205 $$\hat{J}_i = -D_i^{\mathrm{inter}} \frac{\partial \varphi^{\mathrm{s}} C_i^{\mathrm{s}}}{\partial z} - \varphi^{\mathrm{s}} D_i^{\mathrm{intra}} \frac{\partial C_i^{\mathrm{s}}}{\partial z} + \varphi^{\mathrm{s}} w C_i^{\mathrm{s}}.$$

Here, D_i^{inter} and D_i^{intra} are respectively the inter- and intraphase biodiffusion coefficients of the solid i; w is the solids' advection rate. We suppose that the biodiffusion coefficients within a given sediment column are the same for all solids: $D_i^{\mathrm{inter}}(z) \equiv D^{\mathrm{inter}}(z)$ and $D_i^{\mathrm{intra}}(z) \equiv D^{\mathrm{intra}}(z)$. For convenience, we define $D^{\mathrm{bt}}(z) = D^{\mathrm{inter}}(z) + D^{\mathrm{intra}}(z)$ and $D^{\mathrm{inter}}(z) = \beta(z) D^{\mathrm{bt}}(z)$ where $\beta(z)$ sets the interphase fraction of the biodiffusion process ($\beta = 0$ for the intraphase and $\beta = 1$ for the
210 interphase end-members). After application of the chain rule to the derivative in the interphase diffusion term, $\hat{J}_i$ becomes

$$\hat{J}_i = -\varphi^{\mathrm{s}} D^{\mathrm{bt}} \frac{\partial C_i^{\mathrm{s}}}{\partial z} + \left(\varphi^{\mathrm{s}} w - \beta D^{\mathrm{bt}} \frac{\partial \varphi^{\mathrm{s}}}{\partial z} \right) C_i^{\mathrm{s}}. \tag{2}$$

Solutes are transported by molecular and ionic diffusion in porewaters, by interphase bioturbation, porewater advection and by bioirrigation. The complete expression for the local transport term of a porewater solute i would thus write

$$\hat{J}_i = -\varphi^f \frac{D_i^{sw}}{\theta^2} \frac{\partial C_i^f}{\partial z} - D_i^{inter} \frac{\partial \varphi^f C_i^f}{\partial z} + \varphi^f u C_i^f,$$

215   where D_i^{sw} is the free diffusion coefficient of the solute i in seawater, θ^2 is tortuosity, parametrized as function of porosity, and u is the porewater advection rate. Applying the chain rule to the second term on the right-hand side and collecting similar terms, we get

$$\hat{J}_i = -\varphi^f \left(\frac{D_i^{sw}}{\theta^2} + \beta D^{bt} \right) \frac{\partial C_i^f}{\partial z} + \left(\varphi^f u - \beta D^{bt} \frac{\partial \varphi^f}{\partial z} \right) C_i^f.$$

In the absence of impressed flow, transport by porewater advection is, however, negligible compared to diffusion; biodiffusion
220   coefficients are furthermore an order of magnitude lower than molecular and ionic diffusion coefficients. The expression for the local transport term of a porewater solute i adopted in MEDUSA then reduces to

$$\hat{J}_i = -\varphi^f \frac{D_i^{sw}}{\theta^2} \frac{\partial C_i^f}{\partial z}. \tag{3}$$

It should be noticed that in the current version of MEDUSA, neglecting advection and the effect of interphase biodiffusion on solutes contributes to ensure a more precise mass balance. Porewater advection could still be considered for steady-state
225   applications, where $u_{tot} = u - \frac{\beta D^{bt}}{\varphi^f} \frac{\partial \varphi^f}{\partial z}$ would always be oriented downwards. However, in transient simulation experiments, where u may temporarily be oriented upwards (unburial, chemical erosion), porewaters would flow into the REACLAY realm, requiring the knowledge of solute concentrations below the modelled domain. These latter are, however, currently not tracked.

Bioirrigation provides a non-local transport mode for solutes. In MEDUSA, the source-sink approach (Boudreau, 1984) is used to quantify the effect of bioirrigation:

230   $$\hat{Q}_i = \alpha \varphi^f (C_i^{oc} - C_i^f).$$

Here α is the bioirrigation "constant", which may be depth-dependent, and C_i^{oc} the concentration of solute i in the irrigation channels, set equal to the solute's concentration in the seawater overlying the sediment.

Chemical Reactions and Equilibria

The set of chemical reactions and equilibria to consider is completely dependent upon the given application, i.e., on the chemi-
235   cal composition of the sediments required, the diagenetic processes to consider (e.g., organic matter remineralisation, possibly following several pathways, carbonate dissolution, . . .) and the equilibria between components of solute systems (e.g., carbonate, phosphate, borate systems) to take into account. MEDUSA does not include a standard composition and reaction/equilibrium network but must be configured to fit the complexity requirements of a given application: including one or more classes of organic matter (solid or dissolved), one or more types of carbonates, one or more organic matter degradation processes, etc.
240   The chemical interconversion reactions represented by the $\hat{r}_i$ terms in the source-minus-sink term $\hat{S}_i$ are orders of magnitudes faster than all other reactions. They are supposed to evolve in quasi-equilibrium. The $\hat{r}_i$ are therefore eliminated from the

partial differential equation system by considering appropriate linear combinations of selected equations and by including the thermodynamic equilibrium equations in the system of equations. The partial differential equation system is thus converted into a differential algebraic equation system. The subroutines required to evaluate the source and sink terms related to chemical

245 reactions and to convert the complete system to a differential algebraic system are generated by the companion MEDUSA COnfiguration and COde GENeration tool (MEDUSACOCOGEN) described in section 2.4 below.

Additional constraints

The static volume conservation equation is used to replace one of the solids' evolution equations:

$$\sum_{i \in \mathcal{I}^s} \vartheta_i C_i^s = 1. \tag{4}$$

250 Here $\mathcal{I}^s$ denotes the inventory of solid components considered in the model configuration and ϑ_i the partial specific volume of solid i. We suppose that the densities ρ_i of individual solid components are constant and independent of each other. In this case $\vartheta_i = 1/\rho_i$ and the ϑ_i are also constant. However, although the density of each solid constituent is constant, the average density of the solid phase may vary both in space and time as chemical reactions proceed and modify the sediment composition and influence the advection rate profiles. To ensure compatibility with other early diagenesis models that assume that the solid

255 phase has a constant density (both in space and time), all reactive (non inert) solid components can optionally be declared as volumeless.

Boundary conditions

The differential equation systems describing the evolutions of the compositions of the DBL and REACLAY and the TRANLAY realms have to be completed by boundary conditions connecting them to the ovelying seawater, the underlying CORELAY and

260 between each other. Solute concentrations at the top are derived from those in the overlying ocean water ($C_i^f(z_W, t) = C_i^{oc}(t) -$ a Dirichlet boundary condition), prescribed at the top of the DBL if the model set-up includes one and directly at the SWI if not. If a DBL is included in the model setup solute concentrations at the SWI (i.e., at the interface between the DBL and the REACLAY realm) are derived by assuming concentration and flux continuity accross that interface (Cauchy boundary condition). Solids reaching the sea floor are assumed to "rain through" the DBL (if any) and enter the sediment only at the SWI where flux

265 continuity is used as a boundary condition (leading to a Robin boundary condition).

At the bottom of the REACLAY realm, flux continuity is adopted for both solutes and solids. For solutes, this requires the concentration gradient to reduce to zero (Neumann boundary condition) since $u(z) \equiv 0$ is adopted here. For solids, a variety of effective boundary conditions arise – and the types may change in time – depending on whether biodiffusion has vanished there or not and whether the sediment is burying ($w_B^+ > 0$, where w_B^+ denotes the advection rate on the outer side of REACLAY's

270 bottom interface) or eroding ($wz_B^+ < 0$) solid material at the bottom of REACLAY.

2.1.2 TRANLAY and CORELAY

TRANLAY is a TRANsition LAYer that collects the solids leaving REACLAY through the bottom (see Fig. 1). As soon as its thickness exceeds a given threshold value (by default $1\,\mathrm{cm}$) at the end of a time step, one or more new sediment core layers are formed and subtracted from TRANLAY to be transferred to CORELAY, which is managed as a last-in-first-out stack of sediment

275 layers.

In general, material is only preserved in TRANLAY and CORELAY; it is assumed that no chemical reactions take place there. However, we have to make one exception to this rule: reactions that are part of a radioactive decay chain are still taken into account in these two realms to avoid physically unrealistic results. Radioactive material that would have left REACLAY and be returned there later during a chemical erosion event would contribute to create unrealistically young concentrations in

280 REACLAY if radioactive decay would have been temporarily suspended for a more or less extended time.

2.2 Numerical Solution of the Equation System

The differential algebraic system of equations is solved with a finite volume method. For this purpose, the REACLAY and the DBL realms are partitioned into cells (finite volumes) using a so-called vertex-centred grid. Each one of these two realms is overlaid by an irregularly spaced grid of points, called nodes: each node is representative of a cell. The cell boundaries, called

285 vertices, are located midway between adjacent nodes. The concentrations of the considered solute and solid components are evaluated at the nodes, the fluxes between cells at the vertices. The actual grid-point distribution is obtained by a continuously differentiable mapping of a regular grid in order to make sure that the discrete representation of the equation system is consistent and has the same discretisation order than it would have on a regular grid (Hundsdorfer and Verwer, 2003).

The bottom point of the grid that covers REACLAY is always a node. The nature of the topmost point depends on whether

290 a DBL is included or not: if no DBL is included, the topmost interface of REACLAY—the sediment-water interface, SWI— is located at a grid node; if a DBL is included, the interface at the top of REACLAY is mapped onto a grid vertex, defined by a virtual node located above the top of REACLAY and the topmost interior node of REACLAY. Similarly, the bottom of the DBL is located at a vertex of the DBL grid, defined by a virtual node located below the bottom of the DBL and the lowest node inside the DBL (which is most often the top of the DBL). Detailed information about the grid generation can be found in the technical

295 report 'MEDUSA *Technical Reference*' in the Supplement.

In multi-column setups—this would be the most common usage for coupling to biogeochemical cycle models—every sediment column in MEDUSA must have the same number of grid-points, but the spacing and extent of each of these may be different.

2.2.1 Spatial discretisation

300 The discrete version of the evolution equation for a component i in a cell j represented by the node situated at z_j writes

$$\frac{(\hat{C}_i)_j^n - (\hat{C}_i)_j^{n-1}}{\Delta t_n} + \frac{(\hat{J}_i)_{j+\frac{1}{2}}^n - (\hat{J}_i)_{j-\frac{1}{2}}^n}{h_j} - (\hat{S}_i)_j^n = 0 \tag{5}$$

Here, $\Delta t = t_n - t_{n-1}$ and h_j is the distance that separates the vertices $z_{j-\frac{1}{2}} = \frac{1}{2}(z_j + z_{j-1})$ and $z_{j+\frac{1}{2}} = \frac{1}{2}(z_{j+1} + z_j)$. Equation (5) is slightly modified at the bottom-most node where it relates to a half-cell only and one may chose to formally express the mass-balance equations for that half-cell at the representative node (which is actually the bottom node of the grid, resp.), or

305   at some intermediate point between that node and the delimiting vertex. In the absence of a DBL, a similar procedure is adopted at the top-most node.

The numerical schemes adopted in MEDUSA have been selected with the physical meaningfulness of the results in mind. Accordingly, positiveness of the calculated concentration evolutions was deemed indispensable. The discretisation of the advective part of the local transport term in the equations thus requires an upwinding approach. One may chose between a first-order

310   full upwind and a second order exponential fitting scheme, known elsewhere as the Allen-Southwell-Il'in or the Scharfetter-Gummel scheme (Hundsdorfer and Verwer, 2003). It is closely related to the scheme of Fiadeiro and Veronis (1977): on regularly spaced grids both schemes lead to identical discrete forms of the equations. The exponential fitting scheme is, however, better suitable for the flux-conservative finite volume approach on irregularly spaced grids adopted in MEDUSA as it allows for exact mass conservation.

315   Unlike steady-state models, where the solids' advection rate is always oriented downwards relative to the sediment-water interface, MEDUSA has to be able to cope with solids' advection rates that may have any orientation and that may even change their orientation with time. Both upwinding schemes automatically handle this complication.

2.2.2 Solution strategy

The discretisation of the equation systems leads to a coupled non-linear system of equations that is solved iteratively, using a

320   combination of fixed-point and damped Newton-Raphson iterations. Each iteration proceeds in two stages. First, a fixed-point rule is used to update the advection rate profile $w(z)$, using the depth-integrated solid phase volume conservation equation

$$\varphi^{\mathrm{s}}(z)w(z) - \beta(z)D^{\mathrm{bt}}(z)\frac{\partial \varphi^{\mathrm{s}}}{\partial z} = \sum_{i \in \mathcal{I}^{\mathrm{s}}} \vartheta_i \hat{I}_i^{\mathrm{top}} + \int_{z_T}^{z} \sum_{i \in \mathcal{I}^{\mathrm{s}}} \vartheta_i \hat{R}_i(z')\,dz', \tag{6}$$

where $\hat{I}_i^{\mathrm{top}}$ denotes the deposition rate of solid component i per unit surface of total sediment per unit time, entering the surface sediment through the sediment-water interface at the top. The required reaction rate terms are evaluated by using the most recent

325   available concentration profiles (or the initial state). If required, the biodiffusion and bioirrigation coefficients D^{bt}, β and α are also updated at the beginning of this stage. In a second stage concentration profiles are then updated, using a damped Newton scheme (Engeln-Müllges and Uhlig, 1996). The algorithm uses the analytical Jacobian, except for the derivatives of $w(z)$ with respect to the concentrations of the different model components (eqn. 6), which are neglected.

For the initialization of the iterative scheme, a sequence of approaches has been implemented: (1) the state of the previous

330   time step is used; (2) selected solute profiles are initially set homogeneously equal to the boundary values; (3) a continuation method where the partial specific volumes of all non-inert solids are gradually increased from zero to their actual values; (4) a continuation method where the top solid fluxes are gradually increased from zero to their actual given values; (5) a continuation method where reaction rates are gradually increased from zero to their standard values; (6) a continuation method only used

for steady-state calculations where gradually longer time steps are used and (7) a continuation method only used for columns

335 subject to strong chemical erosion, where the amount of eroded material to return to REACLAY is gradually increased to the calculated value. These are adopted in turn until they generate a sequence that fulfils the convergence criterion.

The equation system is not explicitly scaled. The characteristic scales of the components' concentrations, if provided, are nevertheless taken into account in the convergence criterion. For details, please refer to the "MEDUSA *Technical Reference*" in the Supplement.

340 **2.3 Code Organisation**

The MEDUSA common framework includes the subroutines to assemble the equation system and its Jacobian, and to solve the equation system, modules to make available fundamental data (physical constants, unit conversion parameters, etc.), modules to hold the forcing data and the intermediate results. It also provides the core management system for multiple sediment columns, which can be processed in a sequential or a parallel fashion. For parallel processing, Message Passing Interface

345 (MPI) calls are included and can be activated by a pre-processor switch. Three different MPI interfaces are provided: 1D, 2D and 2D×2D, respectively for a sequential linear distribution of the sediment columns, a two-dimensional ordering (typically longitude-latitude) and a hierarchically ordered two-dimensional array of two-dimensional arrays of sediment columns.

In multi-column setups the chemical composition (solids and porewater solutes) must be the same in all the columns. It is nevertheless possible for each organic matter type (solid or solute) to have different C:N:P:O:H ratios in each column. These

350 individual ratios must, however, remain constant with time.

The framework system must be completed with the specific parts required for a particular application to build a working instance of MEDUSA. This includes first of all the requested composition in terms of solids and solutes, the reaction network of the diagenetic processes to consider and the chemical equilibria between components of solute systems. MEDUSA must also be aware of the material characteristics such as densities, molar compositions, and some thermodynamic properties for solid

355 components, or diffusion coefficients for solutes. Rate laws for the different processes under consideration need to be specified.

The information that is required for producing the Fortran code is collected in a series of XML files that define the composition of the sediment and describe the components, processes and equilibria to be considered. These are processed by the MEDUSA COnfigurator and COde GENerator, MEDUSACOCOGEN, to generate as diverse things as modules providing index parameters to address single components by meaningful names, subroutines to calculate molar masses of the components, subroutines

360 to evaluate reaction rates of all the components and the corresponding derivatives with respect to the relevant component concentrations, to modules to assure the I/O to NETCDF files. The complete diagenesis model is bundled into an object library (`libmedusa.a`) to be linked with the application (host model).

2.4 MEDUSACOCOGEN: the MEDUSA COnfigurator and COde GENerator

The *Reference Guide to the Configuration and Code Generation Tool* MEDUSACOCOGEN in the Supplement provides an

365 exhaustive description of the procedure to follow to build a working MEDUSA application. The formats of the required files are described in full detail with commented examples. The library of rate law functions and equilibrium relationships is also

presented in detail. Further information can be found in the example applications provided in the code. Here, we present only a general overview about the functionality of the code generator.

2.4.1 Main Building List

370 The main building list provides the names of the description files of the solids, solutes and solute systems to consider in a particular model configuration, as well as the process and the equilibrium description file names.

2.4.2 Sediment components: solids, solutes and solute systems

Components (solutes or solids) can be of several types and be part of different classes. We distinguish three types of components: *ignored* (default), *normal* or *parameterized* (for solutes only – see below). Evolution equations are only generated for
375 normal components.

Solids actually encompass all the characteristics of solid phase components: their concentrations, their age or production time, their isotopic signatures, ... A solid's description file provides information about its physical and chemical properties, such as intrinsic density, alkalinity content per mole (both mandatory), chemical composition, molar mass (optional). A solid can be part of one of four classes: *basic solid* (default), *(particulate) organic matter*, *solid colour* or *solid production time*. The
380 basic solid class includes all physical solids but organic matter, be they reactive or not. For numerical stability reasons, it is mandatory to include at least one inert solid in the model sediment components, to be flagged as mud. There is a dedicated class for organic matter, offering special functionality. Chemical composition is mandatory for this class and can be set in terms of their C:N:P ratios, from which the actual composition is then derived by CH_2O, NH_3 and H_3PO_4 building blocks, or completely in terms of the C:N:P:O:H composition. The solid's colour class can be used for immaterial (volume-less)
385 properties of solids, such as classical colour tracers or isotopic properties. Each component of this class is linked to another solid from which it inherits physical and chemical properties. For components in the solid's production time class, the code generator produces adequate equations for age (concentration) tracers. These equations follow the Constituent-oriented Age and Residence time Theory, CART, developed by Delhez et al. (1999) and Deleersnijder et al. (2001). The CART approach provides a means to avoid numerical differentiation in the calculated evolution of the age tracer and the age-carrying component
390 (and also between age tracers carried by different components) as the discrete representation of the underlying evolution equations of the age tracer and the age-carrying component have exactly the same structure and thus suffer from the same numerical dispersion. The original theory has been reformulated here in terms of *production time* instead of *age*. Production time is easier to handle than age in the evolution equations used in MEDUSA. That time remains constant in the absence of chemical reactions and mixing whereas age will continue to evolve with time and thus require a sustained virtual advection
395 or reaction, even if the material carrying the age tracer gets transferred to the CORELAY realm (where mixing and reactions are ignored). The amended theory is detailed in the technical report *Early Diagenesis in Sediments. A one-dimensional model formulation* which is included in the Supplement.

As mentioned above, there is a special type of solutes: *parametrized*. For parametrized solutes, no evolution equations are generated. Their description files must therefore include a code snippet to calculate their abundance or to derive their value

400 from specific boundary conditions. Typical examples of parametrized constituents are the calcium concentration, which can

be derived from salinity, or the saturation concentration of CO_3^{2-} with respect to calcite, which can be calculated from the

degree of saturation at the boundary or from the solubility product. The description files of normal solutes must include a code

snippet to calculate its diffusion coefficient in free seawater. Solutes' descriptions must also include their specific alkalinity

content per mole. We only distinguish between two classes of solutes: *basic solute* (default) and *(dissolved) organic matter*.

405 Just like particulate organic matter, dissolved inorganic matter must be characterised by its chemical composition in terms of

its C:N:P(:O:H) ratios. For basic solutes, the chemical composition is optional.

Finally, a *solute system* is a set of solutes that MEDUSA considers as a total sum in the equilibrium calculations. Typical

examples of solute systems are DIC (dissolved inorganic carbon, composed of CO_2, HCO_3^- and CO_3^{2-}) or the borate system

$(B(OH)_3$ and $B(OH)_4^-)$. Solutes that are part of a solute system are considered to be in local chemical equilibrium with each

410 other. Solute system description files simply list the description files of the solute components that make them up. The code

generator internally compiles *Total Alkalinity* as a solute system, based upon the specific alkalinity contents declared in the

solute description files included in the model configuration.

2.4.3 Processes and equilibria

Description files for *processes* include a representation of the underlying chemical reaction that translates its effect on the

415 various model constituents and specify the rate law to apply. MEDUSACOCOGEN currently provides twenty-one different rate

law formulations (actually thirty as several of them have a few variants). Similarly, *equilibrium* description files must include

a representation of the chemical equilibrium and specify the law of mass action to use for it. Expressions for laws of mass

action (equilibrium relationships) require less variety than process rate laws: the four provided library routines cover the most

common cases.

420 Rate laws and laws of mass action are provided in specially formatted Fortran 95 modules (so-called MODLIB files). The

source code of a MODLIB file is preceded by a header (protected by a conditional inclusion pre-compiler directive) that provides

meta-data helping to identify and classify the different parameters required. The module itself defines (1) a derived type

structure that encapsulates the parameter values and relevant component index references and (2) a subroutine to evaluate the

rate-law expression, resp. the equilibrium relationship, for given concentration and parameter values, and the derivatives with

425 respect to the concentrations of the model components. MODLIB files for laws of mass action must further include a subroutine

to set the equilibrium constant (currently derived from the boundary conditions) and another one to evaluate the scale to applied

to the equilibrium relationship. The current collection can be easily extended by adding MODLIB files to the library (for details

about how to do this, please refer to the MEDUSACOCOGEN reference guide in the Supplement).

Chemical equilibria are always taken into account in the DBL and the REACLAY realms. Processes are usually considered only

430 in the REACLAY realm. However, processes involving only solutes can also be considered in the DBL. In addition, processes

that represent radioactive decay of solid trace elements (i.e., of elements whose volume is considered negligible and that do

therefore not impinge on the advection rate profile) should be declared to apply also in the TRANLAY and CORELAY realms

(where reactions are normally stalled). This way, adequate corrections can be applied in case a sediment column becomes

subject to chemical erosion and previously buried material gets remixed into the REACLAY realm. Without such corrections,
435   the material returned to TRANLAY or REACLAY would appear too young.

3   Test Case Applications

Three applications have been selected to illustrate the functionality of MEDUSA: (1) a replication of the ALL simulation
experiment from Munhoven (2007), supplemented with an extended configuration that attaches an age tracer to calcite; (2) a
coupling simulator where the boundary conditions that would normally be provided by a biogeochemical model that MEDUSA
440   would be coupled to are read from a file; (3) a MEDUSA configuration with complex composition and reaction network as
considered in state-of-the-art early diagenesis models used for the analysis of site observational data.

3.1   MEDMBM-PT – Coupled simulation experiment with chemical erosion and resolved sedimentary records

MEDUSA produces truly resolved and, via its CART-based age/production time control system, consistently dated synthetic
sedimentary records. In order to illustrate the potential of this combination of features, the ALL experiment from Munhoven
445   (2007) is repeated here with a MEDUSA configuration equivalent to the one used in that study, extended to attach age control
information to calcite particles.

3.1.1   Application description

Munhoven (2007) used MBM (Multi-Box-Model) coupled to MEDUSA-v1 to explore the implications of the rain ratio changes
proposed to explain the glacial-interglacial atmospheric CO_2 variations (see, e.g., Archer and Maier-Reimer, 1994) for the
450   preservation-dissolution pattern of carbonate over these time scales. MBM is an eleven-box carbon cycle model of the carbon
cycle in the ocean and the atmosphere. The ocean is subdivided into ten reservoirs as a function of depth (surface, intermediate
and deep layers), latitude (low-latitude, northern and southern high latitudes) and ocean basins (Atlantic, Antarctic and Indo-
Pacific. The ocean reservoirs each have a depth distribution derived from the hypsometric curve. MBM calculates the evolutions
of DIC, TA, phosphate (the limiting nutrient) and oxygen in the oceanic reservoirs and pCO_2 in the atmosphere. In addition,
455   $\delta^{13}C$ and $\Delta^{14}C$ are considered for all carbon bearing tracers and fluxes. Organic carbon, calcite and aragonite are produced
by biological activity in the surface reservoirs and settle down to the intermediate and deep reservoirs. Part of the organic
matter gets remineralised in the water column, the rest transferred to the sediment; all of the carbonate rains down to the sea-
floor and enters the sediment. The coupled model includes 304 MEDUSA sediment columns with a 10 cm thick bioturbated
surface mixed-layer, distributed as a function of depth (one column for each 100 m depth interval of sea-floor) over the five
460   ocean basins delimited by the five surface reservoirs (North Atlantic, Equatorial Atlantic, Antarctic, Equatorial Indo-Pacific
and North Pacific). A grid with 21 nodes was used for the sediment columns. The sediment composition is the same as in
Munhoven (2007): the solid phase is composed of clay, calcite, aragonite and organic matter; pore water solutes are CO_2,
HCO_3^-, CO_3^{2-} and O_2 as solutes, the carbonate system being in thermodynamic equilibrium. Here, we further include an
age tracer, carried by calcite. Processes taken into account are calcite and aragonite dissolution as well as oxic organic matter

Calcite dissolution	$\hat{R}_{\mathrm{cdis}} = k_{\mathrm{c}}\,(1-\varphi)\,[\mathrm{Calcite}]\,((1-[\mathrm{CO_3^{2-}}]/C_{\mathrm{cs}})^+)^{4.5}$
	with $k_{\mathrm{c}} = 365.25\,\mathrm{yr}^{-1}\,(=100\,\%\,\mathrm{day}^{-1})$, $C_{\mathrm{cs}} = C_{\mathrm{cs}}(S,T,p)$
Oxic OM remineralisation	$\hat{R}_{\mathrm{omox}} = k_{\mathrm{ox}}\,(1-\varphi)\,[\mathrm{OrgM}]\,([\mathrm{O_2}]/(C_{\mathrm{hox}}+[\mathrm{O_2}]))$
	with $k_{\mathrm{ox}} = 0.024\,\mathrm{yr}^{-1}$, $C_{\mathrm{hox}} = 20\,\mu\mathrm{mol/L}$
Aragonite dissolution	$\hat{R}_{\mathrm{adis}} = k_{\mathrm{a}}\,(1-\varphi)\,[\mathrm{Aragonite}]\,(C_{\mathrm{as}}-[\mathrm{CO_3^{2-}}])^{1.87}$
	with $k_{\mathrm{a}} = 53.8\,\mathrm{yr}^{-1}\,(\mathrm{mol}^{-1}\mathrm{m}^3)^{1.87}$, $C_{\mathrm{as}} = C_{\mathrm{as}}(S,T,p)$

Table 3. Reaction rate law expressions and parameter values used for the MBM experiments. For simplicity, we assume that $1\,\mathrm{L} = 1\,\mathrm{dm}^3$. C_{cs} is the $\mathrm{CO_3^{2-}}$ concentration in seawater at saturation with respect to calcite and C_{as} that for aragonite; C_{hox} is the half-saturation concentration of $\mathrm{O_2}$ for the oxic remineralisation of organic matter. $(\dots)^+$ denotes the positive part of $(\dots)$. The different reaction rates, $\hat{R}$, are expressed in terms of the dissolving/remineralised solid, in $\mathrm{kg}/(\mathrm{m}^3\,\mathrm{total\ sediment})$. Concentrations of solids are expressed in $\mathrm{kg}/(\mathrm{m}^3\,\mathrm{solid\ sediment})$, those of solutes in $\mathrm{mol}/(\mathrm{m}^3\,\mathrm{porewater})$.

465 remineralisation. We make the simplifying assumption that the particles' age does not influence its solubility, which allows for a straightforward generation of the required evolution equation terms by MEDUSACOCOGEN. The exact formulations of the rate laws and the adopted parameter values are given in Table 3. MBM furthermore considers carbonate accumulation on the continental shelf.

The main driving forces in the ALL experiment are (1) the changing shelf accumulation rates, which depend on the extent
470 of low-latitude flooded shelves, which depends in turn on the sea-level whose history is prescribed, (2) the changing export rain ratio (i.e., the carbonate-C to organic-C in the biogenic export fluxes), whose evolution is prescribed as well and which is 40% lower at peak glacial than at peak interglacial times and (3) the riverine $\mathrm{HCO_3^-}$ inputs and atmospheric $\mathrm{CO_2}$ consumption rates, which are derived from Jones et al. (2002). The deep-sea sedimentary accumulation patterns adjust onto the DIC and TA variations induced by these three factors. Please refer to Munhoven (2007) for additional details and references.

475 ### 3.1.2 Results and discussion

Simulation experiments were run over 240,000 yr with cyclically repeated forcings (temperature, sea-level, rain-ratio changes, weathering, etc.) with a 120,000 yr period. Fig. 2 shows two aspects of the surface sedimentary $\mathrm{CaCO_3}$ content. The top panel depicts the actual time-dependent evolution of that content in the sedimentary mixed-layer in the Equatorial Indo-Pacific part of the model ocean (indistinguishable from that shown in Munhoven (2007)). The bottom panel shows the resulting
480 sedimentary record (synthetic cores), where each dot represents a 1 cm thick sample and the crosses depict the composition of the surface mixed layer (the REACLAY realm) as a function of depth, most of which overprint each other as both age and material distributions are rather homogeneous there, especially at depths shallower than 4700 m. It should be noted that the black dots, which correspond to samples almost devoid of the time-carrying calcite component, provide only incomplete or unreliable information and several of these may possibly overprint each other. The white and grey lines in the top panel respectively
485 represent the evolutions of the carbonate compensation depth (CCD, defined here as the depth where the carbonate dissolution
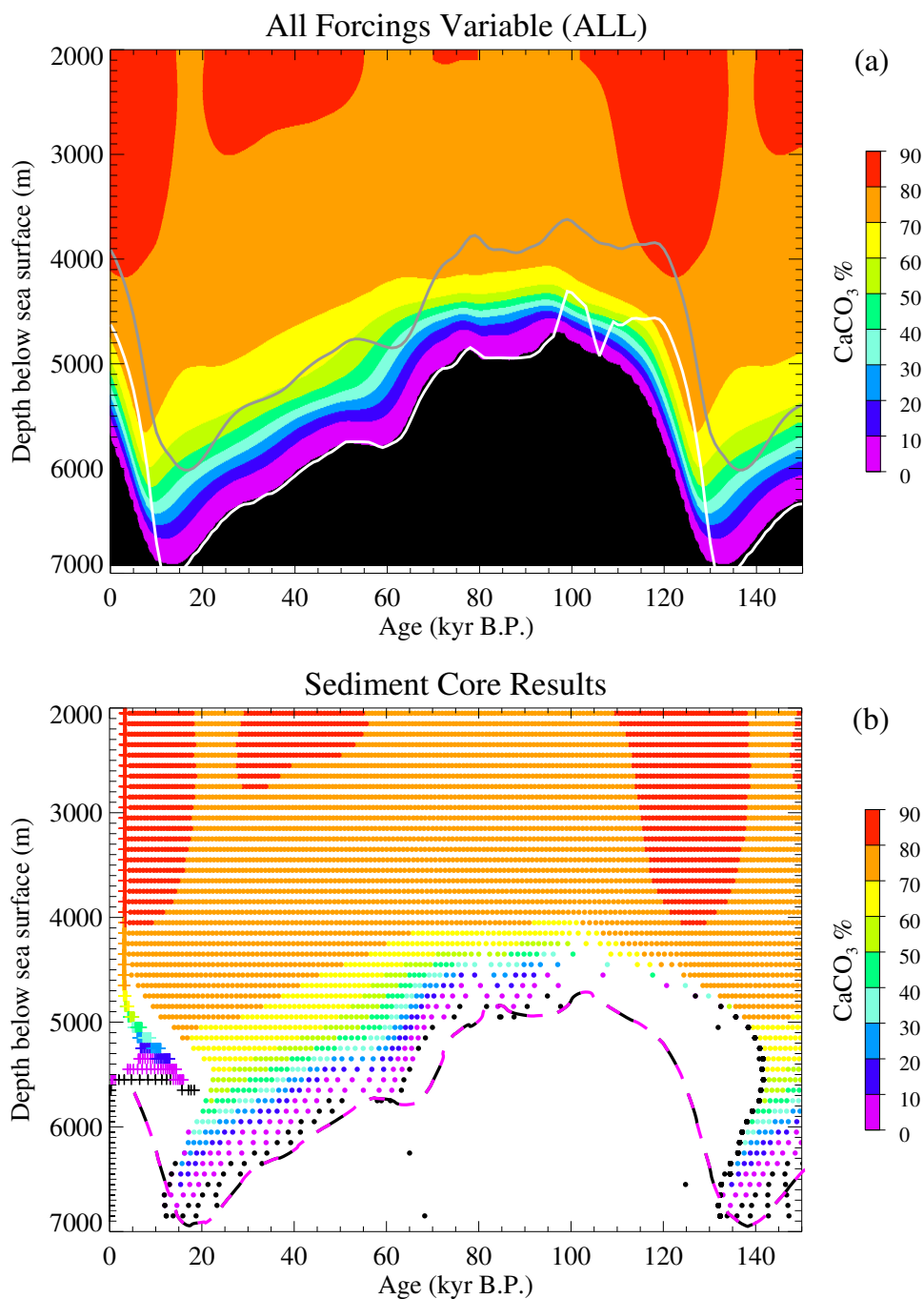
Figure 2. Average surface sediment CaCO₃ content for the ALL experiment from Munhoven (2007). (a) Actual surface sediment %CaCO₃ as a function of time. The grey line traces the evolution of the calcite saturation horizon (CSH), the white line the carbonate compensation depth (CCD) where the dissolution rate equals the deposition rate. (b) Synthetic sediment core record from cores "drilled" at 100 m sea-floor depth intervals from 2050 to 6850 m d.b.s.l. in the low-latitude Indo-Pacific box, as a function of age of the layers. The long dashed line indicates the limit between the black and magenta zones in panel (a), shifted by 5 kyr to the right.

rate is equal to the carbonate deposition rate) and of the calcite saturation horizon (CSH, i.e., the depth at which saturation with respect to calcite is reached). The two distributions are broadly similar but present noticeable differences. There is first of all a systematic time lag of about 3 to 8 kyr, best discernible in the regions where $\%CaCO_3$ exceeds 70%. This time lag is due to the fact that the age tracer tracks the average age of the surface sediment at burial, which is different from zero at all times.

490 Another important difference is the alteration of the actual evolution (Fig. 2a) in the sedimentary record (Fig. 2b). The most striking differences are visible during times of shoaling CCD at depths where $\%CaCO_3$ is lower than 70%. As shown by the long-dashed line on Fig. 2b, which traces the evolution of the limit between the magenta and the black zones from Fig. 2a (the 0% calcite line), shifted by 5 kyr towards the greater ages to account for the average calcite burial age, up to 20 kyr of calcite history have been deleted from the record between 4700 and 6700 m d.b.s.l. due to chemical erosion.

495 MEDUSA always includes at least internally a TRANLAY-CORELAY stack of sediment layers underneath the REACLAY realm in order to handle possible chemical erosion events. These layers can a priori be only approximately dated from the recorded time of burial for each layer, i.e., the time when a given layer is separated from TRANLAY and transferred to CORELAY. With the CART based production time information attached to a solid constituent, this shortcoming can be overcome.

3.2 COUPSIM – Coupling simulator

500 MEDUSA has already been coupled to several ocean biogeochemistry and Earth System Models. First results have been published for the coupling to the Community Earth System Model, CESM (Kurahashi-Nakamura et al., 2020); other coupling projects are well advanced (Moreira Martinez et al., 2016; Völker et al., 2020).

To illustrate the procedure of coupling MEDUSA to a biogeochemical model and to assess the computational cost of a typical sediment module for a real three-dimensional ocean biogeochemistry model, a coupling simulator, COUPSIM, was developed 505 where the boundary conditions that would normally be provided by the host biogeochemical model are read from a file.

3.2.1 Application description

We use results obtained with the coupled Biogeochemistry/Ecosystem/Circulation model, BEC (Moore et al., 2004),[2] that were made publicly available (Moore et al., 2005) in the framework of the Synthesis and Modelling Project of the U.S.-Joint Global Ocean Flux Study (U.S.-JGOFS) research program. That version of BEC consists of a marine ecosystem model coupled 510 to a preliminary version of the Community Climate System Model, CCSM 2.0, Parallel Ocean Program, POP. The coupling simulator was designed to run with annual or multi-annual time steps. The required forcing data were therefore extracted from the provided monthly-mean datasets and aggregated into a yearly average climatology.

A MEDUSA configuration with four solid (clay, calcite, organic matter and opal) and six solute components (CO_2, HCO_3^-, CO_3^{2-}, O_2, NO_3^- and H_4SiO_4) was chosen. The processes considered are calcite dissolution, oxic respiration of organic matter, 515 organic matter degradation by nitrate reduction and full denitrification and opal dissolution. The exact rate law expressions used are given in Table 4. The model sediment columns are supposed to extend over the typical bioturbated mixed-layer depth of about 10 cm throughout, covered by a grid with twenty-one nodes. The vertical resolution of the sediment column is thus of the

---

[2]Later references (e.g., Moore et al., 2013) resolve BEC as "Biogeochemical Elemental Cycling."

Calcite dissolution	$\hat{R}_{\mathrm{cdis}} = k_{\mathrm{c}} \, (1-\varphi) \, [\mathrm{Calcite}] \, ((1-[\mathrm{CO_3^{2-}}]/C_{\mathrm{cs}})^{+})^{4.5}$
	with $k_{\mathrm{c}} = 36.525 \, \mathrm{yr}^{-1} \, (= 10\% \, \mathrm{day}^{-1})$, $C_{\mathrm{cs}} = C_{\mathrm{cs}}(S,T,p)$
Oxic OM remineralisation	$\hat{R}_{\mathrm{omox}} = k_{\mathrm{ox}} \, (1-\varphi) \, [\mathrm{OrgM}] \, ([\mathrm{O_2}]/(C_{\mathrm{hox}} + [\mathrm{O_2}]))$
	with $k_{\mathrm{ox}} = 0.015 \, \mathrm{yr}^{-1}$, $C_{\mathrm{hox}} = 3 \, \mathrm{\mu mol/L}$
OM remin. by nitrate reduction	$\hat{R}_{\mathrm{omnr}} = k_{\mathrm{nr}} \, (1-\varphi) \, [\mathrm{OrgM}] \, ([\mathrm{NO_3^-}]/(C_{\mathrm{hnr}} + [\mathrm{NO_3^-}])) \, (C_{\mathrm{io}}/(C_{\mathrm{io}} + [\mathrm{O_2}]))$
	with $k_{\mathrm{nr}} = 0.005 \, \mathrm{yr}^{-1}$, $C_{\mathrm{hn}} = 30 \, \mathrm{\mu mol/L}$, $C_{\mathrm{io}} = 10 \, \mathrm{\mu mol/L}$
Opal dissolution	$\hat{R}_{\mathrm{odis}} = k_{\mathrm{o}} \, (1-\varphi) \, [\mathrm{Opal}] \, (C_{\mathrm{os}} - [\mathrm{H_4SiO_4}])^{+}$
	with $k_{\mathrm{o}} = 0.05 \, \mathrm{yr}^{-1} \, \mathrm{mol}^{-1} \mathrm{m}^3$, $C_{\mathrm{os}} = 700 \, \mathrm{\mu mol/L}$

Table 4. Reaction rate law expressions adopted for COUPSIM and parameter values for the experiment depicted on Fig. 4 (represented by the full symbols on Fig. 3). Units and notations are the same as in Table 3. In addition, C_{hnr} is the half-saturation concentration of $\mathrm{NO_3^-}$ and C_{io} the characteristic inhibition concentration of $\mathrm{O_2}$ for the oxidation of organic matter by nitrate reduction.

same order as that of the water-column in BEC which has twenty-five vertical layers. MEDUSA sediment columns were attached to sea-floor grid elements at depths greater than $1000 \, \mathrm{m}$ below sea-level, which amounted to 7332 globally. The BEC set-up used by Moore et al. (2004) calls upon a reflective boundary condition at the sea-floor: all of the biogenic material that reaches the bottom-most ocean cells gets entirely remineralised there. Shortcomings of that approach have already been mentioned in the introduction. Here, we have to add another important one: remineralisation or dissolution rates which normally change gradually with depth in the water column present a sudden increase from the second deepest to the deepest layer, often by an order of magnitude, in some instances even by two or more. The dissolution flux in the bottom cells thus has two contributions: one part stems from the dissolution in the water column covered by the bottom cell and one part is related to the reflective boundary condition. To separate these two parts, we therefore extrapolate the water column dissolution flux profile to the bottom cells assuming an exponential decrease with depth, using the values in the two ocean cells overlying each ocean bottom cell. The total bottom dissolution flux is then corrected for this water column dissolution part and the rest is supposed to settle at the seafloor where it enters the surface sediment.

3.2.2 Results and discussion

Reaction rate constants for the different processes have been adjusted in order to derive surface average sediment compositions that come as close as possible to observed distributions. For this adjustment process, the values of the parameters in the dissolution and remineralisation rate laws were varied and the model run to steady-state for each parameter set.

The resulting global distributions of the solid fractions of calcite, total organic carbon and opal (resp. denoted %Calcite, %TOC and %Opal hereafter) were then evaluated against observational data (Seiter et al., 2004) on the basis of their respective standard deviations and correlation coefficients. The results of these experiments are summarised in the Taylor diagram (Taylor, 2001) on Fig. 3. For that diagram each one of the three distributions was normalized with respect to the standard deviation of its respective observational counterpart in order to be able to report all the results on a common scale. The peculiar distributions
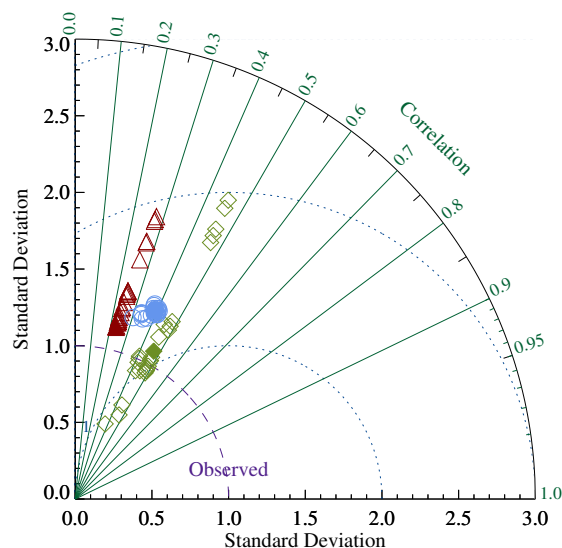
Figure 3. Taylor diagram of the results of the parameter sensitivity experiments carried out with COUPSIM: %Calcite (blue circles); %TOC (green diamonds); %Opal (blue). The full symbols indicate the combination found for the best-fit experiment. Maps for the surface sediment compositions of this best-fit experiment are shown on Fig. 4.

of the different characteristic points on that diagram indicate that there is an structural incompatibility between the data and the possible model results. Calcite points cluster around a correlation coefficient of 0.38 and a standard deviation of 1.3, despite a large range of values (5–1000 %day^{-1}) used for the dissolution rate constant (k_c in Table 4) in the experiments. The opal and organic carbon points align on two beams with correlation coefficient values between 0.23 and 0.27, and between 0.35 and 0.45, respectively, each one with a large range of standard-deviations. For the organic matter dissolution rate laws values between 0.005 and 0.032 yr^{-1} were adopted independently for the two rate constants (k_{ox} and k_{nr} in Table 4); for opal dissolution, rate constant values between 0.04 and 0.07 yr^{-1}, together with asymptotic concentrations ranging between 500 and 700 μmol/L were used (resp. k_o and C_{os} in Table 4).

Among all the experiments carried out, the one that offered the best compromise in terms of standard deviations coming as close as possible to the observations (i.e., to 1 after the normalization) and maximizing the correlation was selected as the best-fit experiment. The corresponding results are represented by the full symbols on Fig. 3. That experiment is characterised by a calcite dissolution rate constant of 36.525 yr^{-1} (i.e., 10 % day^{-1}, only 1/10th of the 100 % day^{-1} of Archer (1991)) for calcite dissolution. For organic matter remineralisation the best-fit rate constants are 0.015 yr^{-1} and 0.005 yr^{-1} for oxic respiration and the oxidation by nitrate reduction, resp. For opal, a comparatively high value of 0.05 yr^{-1} (mol m^{-3})$^{-1}$ had to be adopted in order to avoid widespread opal-dominated sea-floor sediments. For comparison, the rate constant of 30 yr^{-1} of Boudreau (1990) translates to 0.0034 yr^{-1} (mol m^{-3})$^{-1}$ for the rate-law formulation adopted here. The asymptotic ("saturation") con-
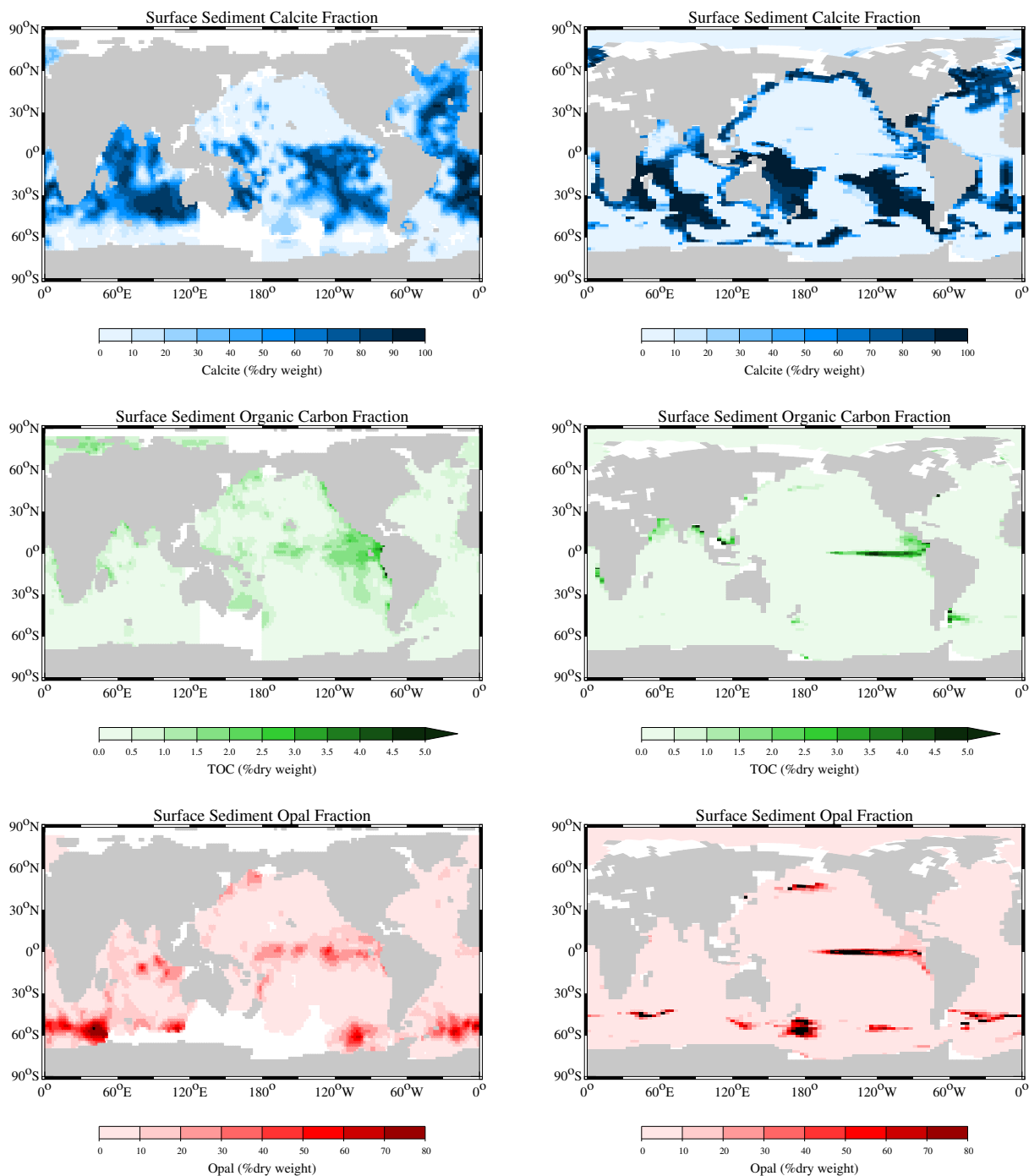
Figure 4. Left column: data (Seiter et al., 2004), binned to a $2° \times 2°$ resolution comparable to the average resolution of BEC; right column: COUPSIM (i.e., MEDUSA forced by the BEC model results of Moore et al. (2004)).

555 centration for opal dissolution had to be set to $700\,\mu M$, which ranges at the cold-water end ($\leq 1\,°C$ of the experimentally derived values of Dixit et al. (2001)).

The resulting average surface model sediment composition at steady state is compared to the target data of Seiter et al. (2004) on Fig. 4. Calcite-rich sediments are produced in the Indian and South Pacific; the calcite-rich sediments along the Atlantic mid-ocean ridge are only reproduced in the South Atlantic and at mid-latitudes in the North Atlantic. The sediments
560 that are richest in TOC are located in the equatorial East Pacific. The opal belt in the Southern Ocean stands out, as well as the maximum in the equatorial East Pacific. This latter is, however, too narrow and similarly to the calcite maxima too sharply delimited.

Among the structural incompatibilities, the band of calcite-rich sediments along the entire rim of the Pacific Ocean in the Northern Hemisphere stands out. These are not seen in the data for the simple reason that the CSH is actually shallower
565 than $1000\,m$ almost everywhere along this band, except in the Sea of Japan (or East Sea) (Yool et al., 2001). In the BEC results, this whole band is supersaturated with respect to calcite. No parameter combination can override this supersaturation and significantly reduce the amount of carbonate preserved. The reflective boundary condition actually contributes to this unrealistic supersaturation, possibly even causes it: as all of the calcite that reaches the deepest ocean cells there unconditionally dissolves the degree of super-saturation of the bottom waters is artificially increased. In the coupled CESM-MEDUSA model
570 experiment of Kurahashi-Nakamura et al. (2020), this carbonate-rich band is not produced. Another important feature of the model %Calcite is the absence of carbonates at the seafloor in the Atlantic north of the equator and south of $30\,°N$, again in contradiction with the data. This results from very low $CaCO_3$ deposition rates of the order of $1–3\,g/m^2/yr$, combined with high lithogenic deposition rates of the order of $15\,g/m^2/yr$ in the BEC results, which caps %Calcite at about 5–15% a priori even in the absence of dissolution. The extended areas of carbonate-rich sea-floor sediments along the North Pacific rim and of
575 strongly diluted sediments in the central Atlantic contribute to the poor correlation coefficient, whatever the model parameter combinations chosen.

In general, the model sediment compositions show far more pronounced contrasts than the observed ones. In all three distributions, the more diffuse features of the global distributions seen in the data are missing. Intermediate values are widespread in the observed distributions, especially for organic carbon where there are only a few isolated spots at the upper end of the
580 depicted range. The model produces in most regions surface sediments that are either poor or extremely rich in calcite. There are only few areas with calcite fractions between 20 and 80 %. The same holds for organic carbon and opal, albeit to a lesser degree for the latter which presents more extended areas with intermediate abundances.

The sharp contrasts for %Calcite can partly be explained by to the vertical grid resolution of the BEC version used by Moore et al. (2004). The CSH in the South Pacific is situated at a depth of about 2.5–3.3 km and at about 3–3.7 km in the Indian Ocean
585 (Yool et al., 2001). At these depths, the vertical resolution of BEC is about 340–450 m. As the transition zone from carbonate-rich to carbonate-poor sediment depths is about 500 m thick there, it is clear that this transition zone cannot be satisfactorily resolved. There are several options to alleviate this shortcoming. The most obvious one is of course to increase the vertical resolution of the host model. The CESM version used by Kurahashi-Nakamura et al. (2020) has sixty vertical levels. Another option would be to call upon sub-grid scale depth profiles and to attach several (two to four) sediment columns to each model

Number of steps	Step length	Wall-clock time (relative units)				
		Serial	MPI-1D (2)	MPI-2D (2)	MPI-1D (4)	MPI-2D (4)
1	∞	0.049	0.034	0.028	0.021	0.020
1	1000 yr	0.028	0.020	0.016	0.012	0.010
10	100 yr	0.17	0.12	0.097	0.079	0.065
100	10 yr	1.0	0.73	0.62	0.47	0.42
1000	1 yr	7.7	5.9	4.8	3.5	3.2

Table 5. Execution times of the COUPSIM best-fit experiment. One unit of CPU time corresponds here to 9:14.73 min. The executing platform had an Ubuntu 16.04.6 LTS operating system (64-bit kernel 4.4.0-185-generic) running on a 1.90 GHz Intel® Core™ i7-8650U CPU; the codes were compiled with GFORTRAN 5.4.0, using optimisation level -O0. Experiments carried out with the MPI interfaces used OPENMPI v. 1.10.2 and were run on as many processes as indicated in brackets.

590   sea-floor grid element. This would of course increase the computational burden of the sediment part of the model, but as can be deduced from the execution times reported and discussed below, these would not represent a major hindrance, given the efficiency of the numerical procedures adopted in MEDUSA.

The %Opal distribution is essentially correlated to the deposition flux rates of opal, which themselves present a highly contrasted distribution. %TOC appears to depend on the organic deposition flux rate and the bottom water oxygen distribution.

595   The preservation tongue in the equatorial East Pacific results from a well delimited deposition rate maximum, in combination with mid to low oxygen concentration rates (20–160 μmol/L). The high organic deposition rates in the Southern Ocean and along the west coasts of Africa do, on the other hand, not lead to high %TOC as these regions are much better oxygenated (160–250 μmol/L).

3.2.3   Execution times

600   The execution times for the best-fit experiment for different computing environments (serial, parallel MPI with the MPI-1D and MPI-2D interfaces) are reported in Table 5. MPI-2DT2D execution times are not reported as they are always within a few percent of those for MPI-2D. The results discussed above were for steady state, i.e., one infinitely long time step. To assess the computational overburden of typical experimental runs, we further added execution times for a 1000 yr simulation experiment, with sediment model steps ranging from 1 to 1000 yr. To allow for an easier comparison, the execution times are reported

605   relative to the serial experiment with 100 time steps of 10 yr which took 9:14.73 min on the computing platform used for the experiments. The usage of one-year time steps makes this serial experiment last 7.7 times longer (1:11:09 hours). Parallel execution allows a considerable reduction of these execution times: with two processors, the execution time of the reference experiment is reduced by 38% and by 68% with four processors (using the MPI-2D interface). Relative reductions are nearly the same for the simulations with a one-year time step. The MPI-1D, which offers the best work-load balance in theory as the

610 sediment columns can be optimally distributed among the processes, is about 10–20% less efficient than the MPI-2D interface, which offers a poorer work-load balance in theory, because of a more complicated coordination overhead. All in all, we may expect that the computational overburden of MEDUSA would represent only a small fraction of the total execution time of a complex Earth System Model.

3.3 JEASIM – Complex composition and reaction network model

615 In order to compare the performance of MEDUSA to that of other state-of-the-art early diagenesis models, we revisited the study of Jourabchi et al. (2008) who used the Biogeochemical Reaction Network Simulator, BRNS (Jourabchi et al., 2005) to analyse sea-floor sediment O_2 and pH profile data from thirteen different sites. The model description in Jourabchi et al. (2008) is sufficiently detailed and complete to allow a meaningful replication.

3.3.1 Application description

620 Here we simplify the original model configuration by neglecting the sulphurous constituents (sulphate and sulphide) and methane as well as the sulphur-based processes (sulphate reduction, sulphide oxidation) and methanogenesis. Jourabchi et al. (2008) found that these were significant at a few sites only (their sites 40, 48 and 120). We furthermore do not explicitly consider H^+ and OH^- but similarly to van Cappellen and Wang (1996), we include their effects implicitly into the combined carbonate and borate equilibria. The adopted model configuration thus includes CO_2, HCO_3^-, CO_3^{2-}, O_2, NO_3^-, Mn^{2+}, Fe^{2+},

625 NH_4^+, $B(OH)_3$ and $B(OH)_4^-$ as solutes, two classes of organic matter, clay, calcite, MnO_2 and $Fe(OH)_3$ as solids. The primary redox reactions considered are organic matter oxidation by oxic respiration, by nitrate reduction and denitrification, by Mn(IV) reduction and by Fe(III) reduction, each one duplicated for the two classes of organic matter. The secondary redox reactions considered are nitrification, Mn^{2+} and Fe^{2+} re-oxidation by O_2 and Fe^{2+} re-oxidation by MnO_2. Furthermore, calcite dissolution is included. The carbonate and borate systems are kept in equilibrium. The resulting application is called

630 JEASIM (Jourabchi Et Al. SIMplified).

Unlike BRNS-GLOBAL, MEDUSA is based upon a complete composition approach with regard to solids: it is assumed that the composition of the solid phase is completely known and the solids' advection rate profile is deduced from the porosity and the reaction rate profiles (see eqn. (6)). Jourabchi et al. (2008) do not consider the effect of chemical reactions on the solid advection rate profile but only set the burial velocity, from which the advection rate profile is then derived, assuming that

635 reactions do not have any influence on the advection rate profile (i.e., the integral term in eq. (6) is neglected). This behaviour can be simulated in MEDUSA by calling upon the *volumeless solids* option at compile time. With this option, only the main inert solid is considered to have a finite density. All the others are considered to be tracers without significant volume, but only mass (i.e., they have zero partial specific volume and infinite density). Both approaches are mathematically equivalent and both have an important drawback: they allow to transport physically unrealistic amounts of non-inert material (e. g., calcite

640 mass fractions exceeding 100%), as we will see below. The model sediment columns were assumed to extend down to 82 cm as in the original study; we used a REACLAY grid with 321 nodes, without a DBL. Porosity and bioturbation profiles were prescribed, using the information provided by Jourabchi et al. (2008). Boundary and forcing conditions (solute concentrations,

calcite saturation state at the SWI, solids' burial rate) were also taken from Jourabchi et al. (2008). For our purpose, the solids' burial rate was converted to an equivalent flux of inert material (dubbed clay) across the SWI.

3.3.2 Adjustment procedures

The adjustment was carried out in two stages, for each of the thirteen stations. At the first stage, the organic matter deposition rate and the degradation rate constants were adjusted in order to reproduce the measured oxygen concentration profiles; calcite dissolution was ignored. For the second stage, these two parameters were held fixed at the values obtained during the first stage. This time, the calcite deposition rate and the calcite dissolution rate constant were adjusted in order to reproduce the measured pH profiles. We only considered calcite dissolution rate orders 1, 2 and 4.5, disregarding the relatively uncommon order 0.5. In contrast to Jourabchi et al. (2008), we did not adopt static initial values for the calcite dissolution rate constant at the second step. We tested random perturbations to these in order allow a deeper exploration of the results space. In a few instances, this allowed us to significantly improve on the results of Jourabchi et al. (2008). Fits were carried out with MPFIT (Markwardt, 2009)[3] with the GNU Data Language (GDL, v. 0.9.6). The minimisation procedure implemented in MPFIT is based upon the Levenberg-Marquardt algorithm. For the pH profile fitting, calculations were based upon H^+ concentrations derived from the pH data.

3.3.3 Results and discussion

O_2 data are comparatively straightforward to fit. The model profiles obtained here are essentially identical to those of Jourabchi et al. (2008) and we are therefore not discussing them here. The detailed results can be found in the `jeasim_vl.ods` spreadsheet file in the `work/jeasim` directory of the code and data archive provided in the Supplement, on the sheet named `jeasim_adj0`; the resulting O_2 profile fits are shown on Figs. S1 and S2 in the *Additional Results* in the Supplement. In terms of the relative misfits, the quality of the fits obtained here is even in most instances slightly superior to those of Jourabchi et al. (2008), except for site 2, where ours is 37% worse. Three others (sites 19, 40 and 59) have similar relative misfits (within $\pm 10\%$ of those of Jourabchi et al. (2008); all the rest present between about 20 and 80% lower relative misfits.

pH profile adjustments, on the other hand, were far less straightforward. We therefore proceeded in several steps (up to three). First, the fitting procedure was carried out with only the pH profile data as a constraint. As mentioned above, the way the application is designed (with the *volumeless solids* option), physically unrealistic mass fractions exceeding 100% cannot be precluded a priori. The fits for six out of the thirteen stations considered (shown on Fig. 5) were affected by this shortcoming. For these stations, the optimal calcite fraction in the total mass entering the sediment column at the SWI ranged between 140 and 5400% (see Table S1 in the *Additional Results* in the Supplement). At sites 19 and 20, the resulting calcite mass fraction in the surface sediment solid fraction was nevertheless physically acceptable; at the four other stations it ranged between 330 and 4100%. For sites 49 and 57 the optimal pH profiles are in poor agreement with the data. The same was observed by Jourabchi et al. (2008): for site 49, they did not even report any pH results and for site 57, they only obtained a profile for the dissolution

---

[3]Available from http://purl.com/net/mpfit.
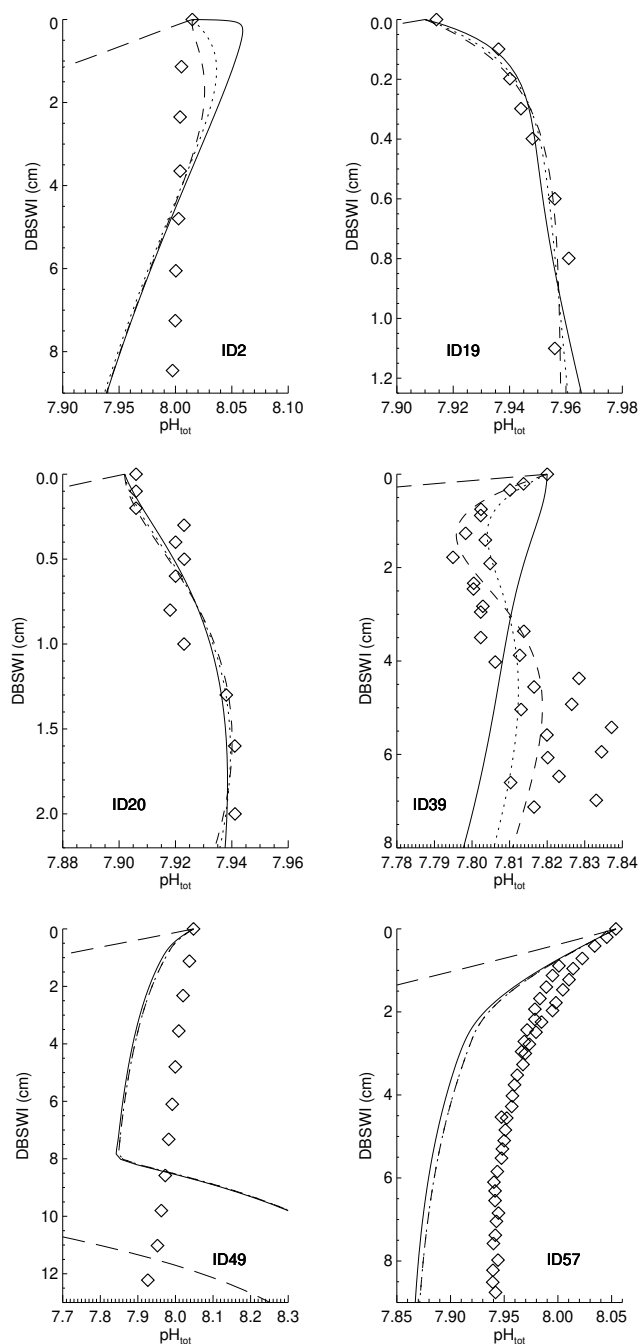
Figure 5. *p*H profiles, unconstrained with respect to the calcite mass fraction in the deposition flux and in the surface solids, for stations that produced physically impossible fits (calcite mass fractions exceeding 100% either in the mass deposition flux or the solids concentration profile). Lines are as follows: long dashed – no calcite dissolution; full – calcite dissolution kinetics of order 4.5; dotted – order 2; short dashes – linear.

rate order 0.5, not considered here. We have been able to derive fits for site 57 for each rate order considered. All of these
675 strongly resemble the profile of Jourabchi et al. (2008) for $n = 0.5$ and also fit the data in a similarly poor way.

For these six sites a second round of fits was performed where the calcite mass fraction in the total deposition flux at the SWI was limited to 90%. The pH profiles from these second fits (except for site 49 which we do not consider any further) together with those of the other sites that passed the first step are shown in Fig. 6. Sites 19 and 20 are again noteworthy as the calcite input limitation does not allow to obtain any meaningful pH profile to fit the data for these. It should, however, be
680 noticed that Jourabchi et al. (2008) also obtained only physically unrealistic results for sites 19 and 20: the calcite deposition flux rates reported for these two sites in their Table 8 would actually require minimum advection rates at the SWI that exceed the prescribed ones by factors of 2.7 to 4.7. For sites 40 and 48, the pH profiles found here are essentially indistinguishable from those of Jourabchi et al. (2008) (although the profiles found for $n = 1$ and $n = 4.5$ at site 48 appear to be swapped). For sites 39 and 58, we find less pronounced subsurface minima than Jourabchi et al. (2008): at site 39, the fits for orders 1 and
685 2 are improved here but degraded for order 4.5; at site 58 all fits are better here as the data do not support well-pronounced subsurface minima. The optimized pH profiles obtained here yield better fits at site 41 for $n = 1$ and $n = 2$, but a worse one for $n = 4.5$. The profile for $n = 4.5$ exhibits too strong a subsurface minimum together with too high pH values at depth. However, attempts to improve the fit of the subsurface minimum deteriorates the quality of the fit at depth, increasing the overall relative misfit. All pH profiles derived here at site 50 are similar to those obtained by Jourabchi et al. (2008) or better. In particular, the
690 profile for $n = 4.5$ does not present a systematic bias towards lower pH values. At site 59, we obtain significantly better pH profile fits. For that site, Jourabchi et al. (2008) had only found pH gradients at the SWI that were opposite to the observations with their model, whereas the gradients obtained here are in agreement with the data (for all calcite dissolution rate orders). For site 120, finally, our pH profiles do not present the bias towards low pH witnessed by the results of Jourabchi et al. (2008). They rather present a bias towards higher pH, caused by the three outliers between 2.5 and 3 cm depth: additional experiments
695 (not shown) where these outliers were removed allowed to improve the relative misfit by a factor of four. In addition, we have also been able to produce a pH profile for $n = 4.5$.

Upon inspection of the other characteristics of the resulting model sediment, we found that most of the sites presented far too low calcite mass fractions in the surface sediment (see Table S2 in the *Additional Results* in the Supplement). Only at sites 39 and 57 does it come close to the observed 90%. This is, however, most likely due to the imposed deposition flux with 90%
700 calcite at these sites. In a third step, we have therefore repeated the experiments for all the sites by adding the surface sediment calcite mass fraction as constraint, letting the mass fraction of calcite in the deposition flux float again. For this purpose, the calcite fractions reported by Jourabchi et al. (2008, Table 1) were assumed to hold for the average over the top 10 cm of the sediment. The resulting pH profiles are shown on Fig. 7. The profiles obtained for sites 2, 19 and 20 require, once more, a few comments. They all apparently present more or less acceptably fitted pH profiles, only slightly worse than at the first
705 step (Fig. 5), but far better than at the second step (Fig. 6). However, the constraint on the surface sediment mass fraction of calcite is unfortunately not sufficient to yield physically realistic results at these three sites. The calculated optimal calcite mass fractions in the deposition flux for all dissolution rate orders range from 140 to 730%, except for site 2, where $n = 1$ and $n = 2$ provide acceptable results, but not $n = 4.5$ (see Table S3 in the *Additional Results* in the Supplement). There is little
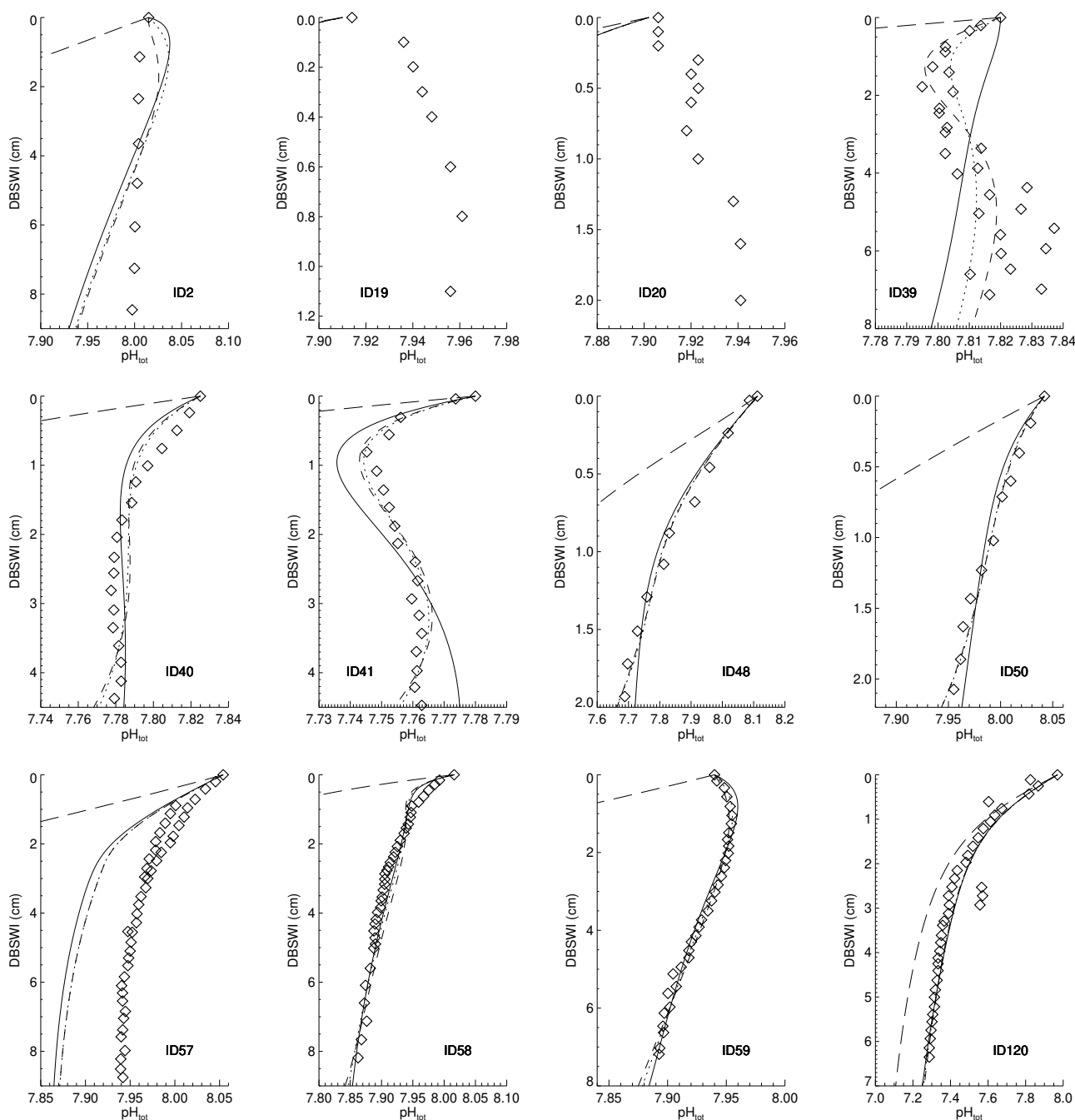
Figure 6. pH profiles for experiments with calcite mass fractions in the deposition flux limited to 90%. Lines are as follows: long dashed – no calcite dissolution; full – calcite dissolution kinetics of order 4.5; dotted – order 2; short dashes – linear.
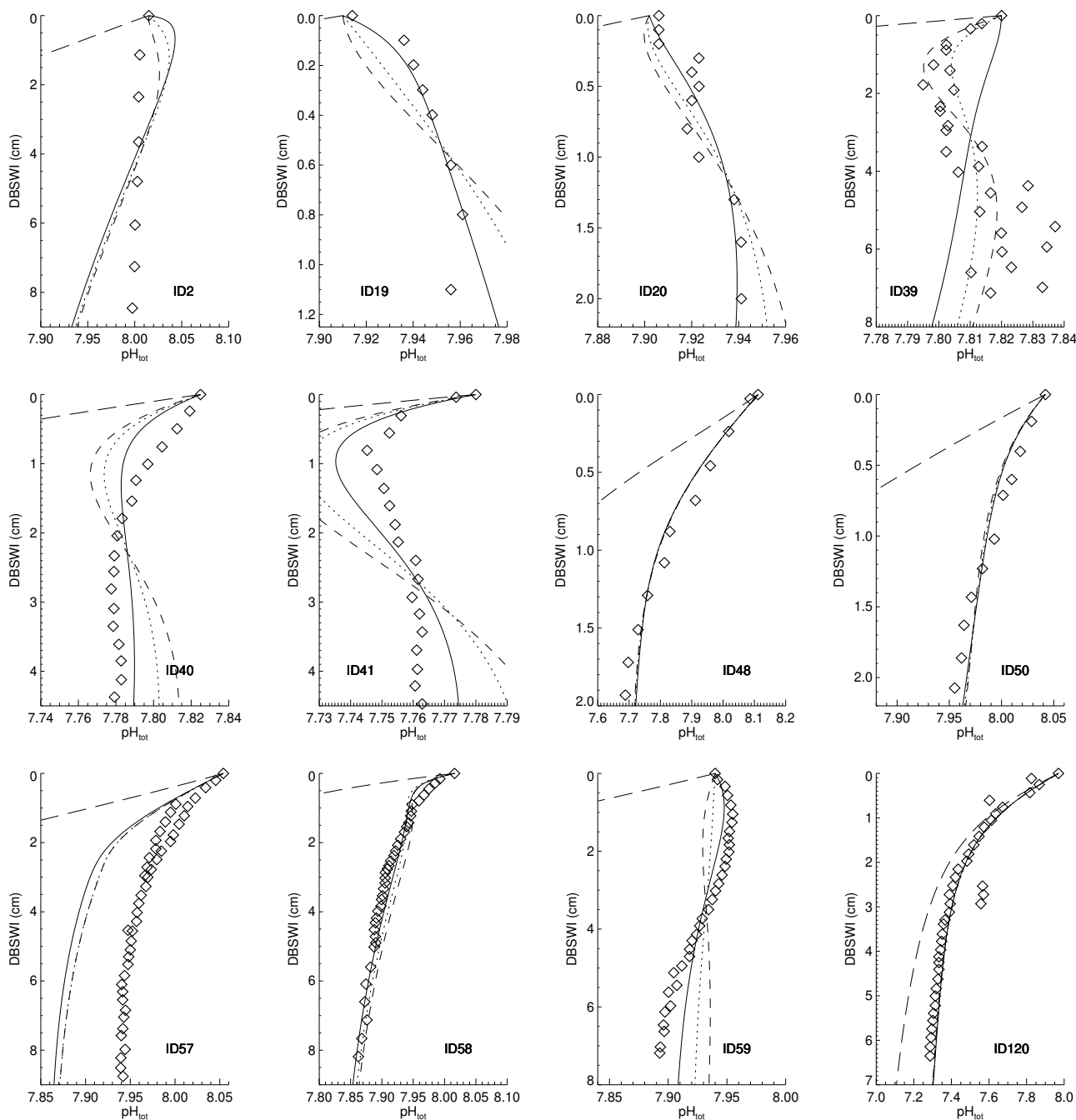
Figure 7. *p*H profiles with data-constrained surface sediment %calcite. Lines are as follows: long dashed – no calcite dissolution; full – calcite dissolution kinetics of order 4.5; dotted – order 2; short dashes – order 1 (linear). Please notice that the $n = 4.5$ fit at site 2 and all the fits for sites 19 and 20 require calcite mass fractions in the deposition fluxes exceeding 100% (between 140 and 730%).

difference between the fits with the limited calcite deposition flux at sites 39, 48, 50, 57, 58 and 120. At site 59, for which
710   the optimal pH profiles obtained at the previous step were superior to those obtained by Jourabchi et al. (2008), the gradients
change now sign for $n = 1$ and $n = 2$ and the quality of the fits degrades; the quality of the profile obtained for $n = 4.5$ is also
sightly degraded but remains acceptable. At site 41, finally, the differences are comparatively large, except for $n = 4.5$. The
reason for these contrasting changes are simple. The target %Calcite is 87%. During the first fitting exercise, the %Calcite was
77% for $n = 4.5$, but only 0.04% and 0.06% for $n = 2$ and $n = 1$, resp. Accordingly, these latter cases require strong increases
715   in the calcite deposition rate combined with strongly reduced dissolution rates to meet that imposed constraint. All in all, we
find that the two models produce results in agreement with each other. Interestingly, the stations for which Jourabchi et al.
(2008) diagnosed a significant role for sulphur-based processes yield optimal pH profiles here that are essentially identical than
the original ones. This should, however, not be seen as a proof that sulphate reduction and subsequent sulphide oxidation are
negligible at the sites under study. It should indeed not be forgotten that the O_2 and pH data profiles only cover the uppermost
720   parts of the sediment porewaters, in some instances only the top-most 1–2.5 cm: for O_2 these are the profiles at sites 2, 19, 20,
48 and 50, for pH those at sites 19, 20, 48 and 50. They do thus provide only a weak constraint on the deeper parts of modelled
sediment depth, where sulphate reduction fuelled processes typically take place.

    Although it would certainly be interesting to investigate the reasons for the failure to produce satisfactory fits to the pH
data profiles with our models, this would go beyond the scope of this model description paper. Besides the simplifications in
725   the sediments compositions and the reaction network, there remain a few differences between BRNS-GLOBAL and the JEASIM
application of MEDUSA and between the adopted fitting procedures. We believe that the differences between the two models
only have minor impact. BRNS-GLOBAL takes the porewater advection into account, whereas MEDUSA does not by default
(as adopted here), since it is small compared to diffusive transport. The fitting procedures may have a more important impact.
The optimisation routine used by Jourabchi et al. (2008) calls upon a simplex algorithm; MPFIT uses a Levenberg-Marquardt
730   method and furthermore allows to take range constraints for the solutions into account. Both algorithms are iterative and suffer
from inherent shortcomings. It is well-known that the simplex method may converge to non-stationary points. With MPFIT
we have experienced situations, where we had to increase the a priori physically sufficient lower boundary of zero to some
non-zero positive value. The iterations eventually "bounced" upon this non-zero value and made the procedure converge to
some well-pronounced minimum, whereas the theoretically sufficient bound of zero would have made the iterations converge
735   to some random low value, producing χ^2 values far above the potential minimum. Furthermore, it should be noticed that we
have carried out the pH fitting on the corresponding H^+ concentrations, whereas Jourabchi et al. (2008) used the pH values
instead. H^+ concentrations offer a far larger dynamical range than pH, thus providing a stronger constraint.

    We concur with Jourabchi et al. (2008) in concluding that there are probably other constituents, reactions and processes not
considered in our models that may significantly impinge on the proton exchange reactions and thus influence the pH profiles
740   in a way that can thus not be reproduced. However, there are additional assumptions that must also be considered to explain
the model-data discrepancies. The empirical relationship used to derive the burial rate from the sea-floor depth is possibly

unreliable for usage at isolated sites. At some stations, a model configuration with a DBL might be required. This is almost certainly the case at site 120, for which Wenzhöfer et al. (2001) have made out a DBL thickness of $725 \pm 25\,\mu\mathrm{m}$.[4]

4   Conclusions

745   In its version 2 MEDUSA, the Model of Early Diagenesis in the Upper Sediment with Adaptable complexity, offers a flexible approach to develop tailored sediment modules suitable for coupling to ocean biogeochemical cycle models, but also for process analysis and teaching. MEDUSA is based upon the standard time-dependent diagenetic equation (e.g., Berner, 1980; Boudreau, 1997) with the vertical as the only spatial dimension. The chemical composition of the solid and solute phases can be chosen to fit the requirements of the scientific question to address. The network of diagenetic reactions (redox processes, min-

750   eral dissolution, . . .) and chemical equilibria in the porewaters can be made exactly as complex as required. The Application Programming Interfaces (APIs) allow the coupling to the most commonly encountered geographical grid layouts in biogeochemical models (unstructured, two-dimensional, or hierarchically ordered two-dimensional arrays of two-dimensional areas). They have furthermore been designed so that existing model configurations can be easily extended (or simplified). The adopted numerical procedures allow for large range of time steps, making MEDUSA suitable for long simulation experiments with well-

755   resolved representations of the sea-floor (several thousands of sediment columns). Parallel processing for multi-column set-ups is supported via Message Passing Interface (MPI) instructions that can be optionally activated.

Three test case applications have been selected and presented in this model description paper. The first one revisits the study of Munhoven (2007) which used the predecessor version MEDUSA-v1. A model configuration with exactly the same functionality as MEDUSA-v1 was set up and extended by the age monitoring facilities offered by MEDUSA. These latter are based

760   upon the Constituent-oriented Age and Residence time Theory, CART (Deleersnijder et al., 2001; Delhez et al., 1999), which has a well-established record in the analysis of geophysical fluid flow models. CART can be easily transposed to the standard equations describing the early diagenesis of seafloor sediments. The newly generated model code accurately reproduces the original results. The added age-control information provides insight into the relationship between the actual time-dependent evolution of the sea-floor sedimentary mixed-layer composition and the resulting sedimentary record.

765   For the second application, a coupling simulator was developed to illustrate the opportunities and to assess the computational requirements of using a fully coupled vertically resolved early diagenesis model as the ocean-sediment exchange scheme in a model of ocean biogeochemical cycles. MEDUSA offers attractive flexibility requiring reasonable computational overburden. MPI interfaces allow for a significant gain in computing time. Even fully coupled simulation experiments with a horizontal resolution of $1° \times 1°$, with of the order of 40,000 sea-floor grid points are conceivable. MEDUSA is thus well suited to upgrade

770   commonly used category 1, 2 and 3 ocean-sediment exchange schemes in biogeochemical models.

The third application considered a complex composition and reaction network. We analyse and compare the performance of MEDUSA to that of the state-of-the-art early diagenesis model BRNS-GLOBAL (Jourabchi et al., 2005) by revisiting the

---

[4]Site 120 is identical to site GeoB4901 in Wenzhöfer et al. (2001).

study of Jourabchi et al. (2008). In that study, porewater O_2 and pH microelectrode profiles taken in situ were interpreted with BRNS-GLOBAL. The results obtained with MEDUSA compare favourably to those obtained by Jourabchi et al. (2008).

775   Like most models MEDUSA has, and will probably always have, a touch of a "never-ending story." In one of the next stages, adsorption processes will be added to MEDUSACOCOGEN. The currently generated model code can be manually amended or patched to take into account adsorption along the lines developed by Berner (1976). A consistent and mechanistically based approach with as few early-stage simplifying assumptions as possible would nevertheless be preferable and a treatment similar to the solute systems is currently being worked out. It is furthermore planned to improve the computing time requirements

780   by dealing separately with variables that do not have any impact on the solids' advection rate profiles. In general, isotopic signatures, production times, colour tracers, etc. range among these variables. This way, the dimensions of the equation system that must be solved for each outer (fixed-point) iteration can be reduced. Currently the computational demand roughly scales as the square of the number of components considered. Thus, even a 10% reduction in the number of components to consider for the complete system of equations would reduce the overall computational demand by about 20%. The remaining variables

785   can then be treated without any further outer iterations once the advection rate profile has stabilised.

The numerical efficiency of MEDUSA allows for long simulation experiments required to analyse the dynamics of development of particular sedimentary features that take a long time to develop. Such features show up in steady-state simulations, but would go undetected in time-dependent simulation experiments unless run over a sufficiently long time. With interactive sediments, a biogeochemical model generally requires much longer to reach equilibrium (50 to 200 kyr). Isotope-enabled ap-

790   plications generally range at the upper end of the range. Vertically resolved early diagenesis models are often of similar vertical complexity (in terms of the number of vertical layers) than the biogeochemical models that they are meant to be coupled to. It is therefore important to have a model that offers the possibility of long time steps, and that can be trimmed down to the bare essentials required by any given application.

Code availability.   The codes used in this paper are provided in the archive included in the Supplement for use under the GNU Affero General

795   Public License, version 3 or later (the μXML library, MEDUSA, MEDUSACOCOGEN and the MEDUSA applications, including MEDMBM) or the Apache-2.0 license (LIBTHDYCT). That archive also includes the required forcing data, except for the data from the coupling simulator, which have to be downloaded from their original sources. Instructions about how to repeat all the reported simulation experiments are given in the *Building and Running the Test Case Applications* Memo in the Supplement.

Author contributions.   GM developed the model and all of its dependencies, designed and carried out the model experiments, performed the

800   analysis of the results, created all the graphics and wrote the paper.

Competing interests.   The author declares that there is no conflict of interest.

Acknowledgements. I thank Parisa Jourabchi and Christof Meile for discussions on their working assumptions and for completing the data used in Jourabchi et al. (2008); Thanks are also due to J. Keith Moore and his colleagues for making the results of their BEC simulation experiments openly available to the public. Financial support for this work was provided by the Belgian Fund for Scientific Research – F.R.S.-FNRS (project SERENATA, grant CDR J.0123.19). Guy Munhoven is a Research Associate with the Belgian Fund for Scientific Research – F.R.S.-FNRS.

805

References

Archer, D.: A data-driven model of the global calcite lysocline, Global Biogeochem. Cy., 10, 511–526, https://doi.org/10.1029/96GB01521, 1996a.

Archer, D. and Maier-Reimer, E.: Effect of deep-sea sedimentary calcite preservation on atmospheric CO_2 concentration, Nature, 367, 260–263, https://doi.org/10.1038/367260a0, 1994.

Archer, D., Winguth, A., Lea, D., and Mahowald, N.: What Caused the Glacial-Interglacial Atmospheric $p$$CO_2$ Cycles ?, Rev. Geophys., 38, 159–189, https://doi.org/10.1029/1999RG000066, 2000.

Archer, D., Morford, J. L., and Emerson, S. R.: A model of suboxic sedimentary diagenesis suitable for automatic tuning and gridded domains, Global Biogeochem. Cy., 16, 1017, https://doi.org/10.1029/2000GB001288, 2002.

Archer, D. E.: Modeling the Calcite Lysocline, J. Geophys. Res., 96, 17 037–17 050, https://doi.org/10.1029/91JC01812, 1991.

Archer, D. E.: An atlas of the distribution of calcium carbonate in sediments of the deep sea, Global Biogeochem. Cy., 10, 159–174, https://doi.org/10.1029/95GB0301, 1996b.

Arndt, S., Regnier, P., Goddéris, Y., and Donnadieu, Y.: GEOCLIM *reloaded* (v 1.0): a new coupled earth system model for past climate change, Geosci. Model Dev., 4, 451–481, https://doi.org/10.5194/gmd-4-451-2011, 2011.

Berner, R. A.: Inclusion of adsorption in the modelling of early diagenesis, Earth Planet. Sc. Lett., 29, 333–340, https://doi.org/10.1016/0012-821X(76)90137-0, 1976.

Berner, R. A.: Early Diagenesis. A Theoretical Approach, Princeton Series in Geochemistry, Princeton University Press, Princeton, NJ, 1980.

Boudreau, B. P.: On the equivalence of non-local and radial-diffusion models for porewater irrigation, J. Mar. Res., 42, 731–735, https://doi.org/10.1357/002224084788505924, 1984.

Boudreau, B. P.: The Mathematics of Tracer Mixing in Sediments : I. Spatially-Dependent, Diffusive Mixing, Am. J. Sci., 286, 161–198, https://doi.org/10.2475/ajs.286.3.161, 1986.

Boudreau, B. P.: Asymptotic forms and solutions of the model for silica-opal diagenesis in bioturbated sediments, J. Geophys. Res., 95, 7367–7379, https://doi.org/10.1029/JC095iC05p07367, 1990.

Boudreau, B. P.: Is burial velocity a master parameter for bioturbation ?, Geochim. Cosmochim. Ac., 58, 1243–1249, https://doi.org/10.1016/0016-7037(94)90378-6, 1994.

Boudreau, B. P.: Diagenetic Models and Their Implementation, Springer-Verlag, Berlin, https://doi.org/10.1007/978-3-642-60421-8, 1997.

Boudreau, B. P.: Mean mixed depth of sediments : The wherefore and the why, Limnol. Oceanogr., 43, 524–526, https://doi.org/10.4319/lo.1998.43.3.0524, 1998.

Brovkin, V., Ganopolski, A., Archer, D., and Munhoven, G.: Glacial CO_2 cycle as a succession of key physical and biogeochemical processes, Clim. Past, 8, 251–264, https://doi.org/10.5194/cp-8-251-2012, 2012.

Bruckner, T., Bashmakov, I. A., Mulugetta, Y., Chum, H., De la Vega Navarro, A., Edmonds, J., Faaij, A., Fungtammasan, B., Garg, A., Hertwich, E., Honnery, D., Infield, D., Kainuma, M., Khennas, S., Kim, S., Nimir, H. B., Riahi, K., Strachan, N., Wiser, R., and Zhang, X.: Energy Systems, in: Climate Change 2014: Mitigation of Climate Change. Contribution of Working Group III to the Fifth Assessment Report of the Intergovernmental Panel on Climate Change, edited by Edenhofer, O., Pichs-Madruga, R., Sokona, Y., Minx, J. C., Farahani, E., Kadner, S., Seyboth, K., Adler, A., Baum, I., Brunner, S., Eickemeier, P., Kriemann, B., Savolainen, J., Schlömer, S., von Stechow, C., and Zwickel, T., chap. 7, Cambridge University Press, Cambridge (UK) and New York (USA), https://www.ipcc.ch/site/assets/uploads/2018/02/ipcc_wg3_ar5_chapter7.pdf, 2014.

Deleersnijder, E., Campin, J.-M., and Delhez, E. J. M.: The concept of age in marine modelling — I. Theory and preliminary model results, J. Marine Syst., 28, 2503–2517, https://doi.org/10.1016/S0924-7963(01)00026-4, 2001.

Delhez, E. J. M., Campin, J.-M., Hirst, A. C., and Deleersnijder, E.: Toward a general theory of the age in ocean modelling, Ocean Model., 1, 17–27, https://doi.org/10.1016/S1463-5003(99)00003-7, 1999.

Dixit, S., Van Cappellen, P., and van Bennekom, A. J.: Processes controlling solubility of biogenic silica and pore water build-up of silicic acid in marine sediments, Mar. Chem., 73, 333–352, https://doi.org/10.1016/S0304-4203(00)00118-3, 2001.

Eby, M., Zickfeld, K., Montenegro, A., Archer, D., Meissner, K. J., and Weaver, A. J.: Lifetime of Anthropogenic Climate Change : Millennial Time Scales of Potential CO_2 and Surface Temperature Perturbations, J. Climate, 22, 2501–2511, https://doi.org/10.1175/2008JCLI2554.1, 2009.

Eby, M., Weaver, A. J., Alexander, K., Zickfeld, K., Abe-Ouchi, A., Cimatoribus, A. A., Crespin, E., Drijfhout, S. S., Edwards, N. R., Eliseev, A. V., Feulner, G., Fichefet, T., Forest, C. E., Goosse, H., Holden, P. B., Joos, F., Kawamiya, M., Kicklighter, D., Kienert, H., Matsumoto, K., Mokhov, I. I., Monier, E., Olsen, S. M., Pedersen, J. O. P., Perrette, M., Philippon-Berthier, G., Ridgwell, A., Schlosser, A., Schneider von Deimling, T., Shaffer, G., Smith, R. S., Spahni, R., Sokolov, A. P., Steinacher, M., Tachiiri, K., Tokos, K., Yoshimori, M., Zeng, N., and Zhao, F.: Historical and idealized climate model experiments: an intercomparison of Earth system models of intermediate complexity, Clim. Past, 9, 1111–1140, https://doi.org/10.5194/cp-9-1111-2013, 2013.

Engeln-Müllges, G. and Uhlig, F.: Numerical Algorithms with Fortran, Springer-Verlag, Berlin, 1996.

Fiadeiro, M. E. and Veronis, G.: On weighted-mean schemes for the finite difference approximation to the advection-diffusion equation, Tellus, 29, 512–522, https://doi.org/10.1111/j.2153-3490.1977.tb00763.x, 1977.

Gehlen, M., Bopp, L., Emprin, N., Aumont, O., Heinze, C., and Ragueneau, O.: Reconciling surface ocean productivity, export fluxes and sediment composition in a global biogeochemical ocean model, Biogeosciences, 3, 521–537, https://doi.org/10.5194/bg-3-521-2006, 2006.

Heinze, C. and Maier-Reimer, E.: The Hamburg Oceanic Carbon Cycle Circulation Model Version "HAMOCC2s" for long time integrations, Technical Report 20, Deutsches Klimarechenzentrum, Hamburg (DE), https://doi.org/10.2312/WDCC/DKRZ_Report_No20, https://www.dkrz.de/mms/pdf/reports/ReportNo.20.pdf, 1999.

Heinze, C., Maier-Reimer, E., and Winn, K.: Glacial p_{CO_2} reduction by the World Ocean : Experiments with the Hamburg Carbon Cycle Model, Paleoceanography, 6, 395–430, https://doi.org/10.1029/91PA00489, 1991.

Heinze, C., Maier-Reimer, E., Winguth, A. M. E., and Archer, D.: A global ocean sediment model for long-term climate studies, Global Biogeochem. Cy., 13, 221–250, https://doi.org/10.1029/98GB02812, 1999.

Heinze, C., Kriest, I., and Maier-Reimer, E.: Age offsets among different biogenic and lithogenic components of sediment cores revealed by numerical modeling, Paleoceanography, 24, PA4214, https://doi.org/10.1029/2008PA001662, 2009.

Hoffert, M. I., Callegari, A. J., and Hsieh, C.-T.: A Box-Diffusion Carbon Cycle Model with Upwelling, Polar Bottom Water Formation and a Marine Biosphere, in: Carbon Cycle Modelling, edited by Bolin, B., vol. 16 of *SCOPE*, pp. 285–305, John Wiley & Sons, Chichester, NY, https://scope.dge.carnegiescience.edu/SCOPE_16/SCOPE_16_1.5.08_Hoffert_287-305.pdf, 1981.

Hülse, D., Arndt, S., Wilson, J. D., Munhoven, G., and Ridgwell, A.: Understanding the causes and consequences of past marine carbon cycling variability through models, Earth Sci. Rev., 171, 349–382, https://doi.org/10.1016/j.earscirev.2017.06.004, 2017.

Hundsdorfer, W. and Verwer, J.: Numerical Solution of Time-Dependent Advection-Diffusion-Reaction Equations, Springer Series in Computational Mathematics, Springer, Berlin, https://doi.org/10.1007/978-3-662-09017-6, 2003.

Ilyina, T., Six, K. D., Segschneider, J., Maier-Reimer, E., Li, H., and Núñez-Riboni, I.: Global ocean biogeochemistry model HAMOCC : Model architecture and performance as component of the MPI-Earth system model in different CMIP5 experimental realizations, J. Adv. Model. Earth Syst., 5, 287–315, https://doi.org/10.1029/2012MS000178, 2013a.

Ilyina, T., Wolf-Gladrow, D., Munhoven, G., and Heinze, C.: Assessing the potential of calcium-based artificial ocean alkalinization to mitigate rising atmospheric CO_2 and ocean acidification, Geophys. Res. Lett., 40, 5909–5914, https://doi.org/10.1002/2013GL057981, 2013b.

Jones, I. W., Munhoven, G., Tranter, M., Huybrechts, P., and Sharp, M. J.: Modelled glacial and non-glacial HCO_3^-, Si and Ge fluxes since the LGM : little potential for impact on atmospheric CO_2 concentrations and a potential proxy of continental chemical erosion, the marine Ge/Si ratio, Global Planet. Change, 33, 139–153, https://doi.org/10.1016/S0921-8181(02)00067-X, 2002.

Jourabchi, P., Van Cappellen, P., and Regnier, P.: Quantitative interpretation of pH distributions in aquatic sediments : A reaction-transport modeling approach, Am. J. Sci., 305, 919–956, https://doi.org/10.2475/ajs.305.9.919, 2005.

Jourabchi, P., Meile, C., Pasion, L. R., and Van Cappellen, P.: Quantitative interpretation of pore water O_2 and pH distributions in deep-sea sediments, Geochim. Cosmochim. Ac., 72, 1350–1364, https://doi.org/10.1016/j.gca.2007.12.012, 2008.

Keir, R. S.: Dissolution of calcite in the deep-sea : theoretical prediction for the case of uniform size particles settling into a well-mixed sediment, Am. J. Sci., 282, 193–236, https://doi.org/10.2475/ajs.282.3.193, 1982.

Keir, R. S.: On the Late Pleistocene Ocean Geochemistry and Circulation, Paleoceanography, 3, 413–445, https://doi.org/10.1029/PA003i004p00413, 1988.

Keir, R. S. and Berger, W. H.: Atmospheric CO_2 content in the last 120,000 years : The phosphate-extraction model, J. Geophys. Res., 88, 6027–6038, https://doi.org/10.1029/JC088iC10p06027, 1983.

Kurahashi-Nakamura, T., Paul, A., Munhoven, G., Merkel, U., and Schulz, M.: Coupling of a sediment diagenesis model (MEDUSA) and an Earth system model (CESM1.2): a contribution toward enhanced marine biogeochemical modelling and long-term climate simulations, Geosci. Model Dev., 13, 825–840, https://doi.org/10.5194/gmd-13-825-2020, 2020.

Luff, R. and Moll, A.: Seasonal dynamics of the North Sea sediments using a three-dimensional coupled sediment-water model system, Cont. Shelf Res., 24, 1099–1127, https://doi.org/10.1016/j.csr.2004.03.010, 2004.

Luff, R., Wallmann, K., Grandel, S., and Schlüter, M.: Numerical modeling of benthic processes in the deep Arabian Sea, Deep-Sea Res. Pt. II, 47, 3039–3072, https://doi.org/10.1016/S0967-0645(00)00058-8, 2000.

Maier-Reimer, E.: Towards a global ocean carbon model, in: Interactions between Climate and Biosphere, edited by Lieth, H., Fantechi, R., and Schnitzler, H., vol. 3 of *Progress in Biometeorology*, pp. 295–310, Swets & Zeitlinger, Lisse (NL), 1984.

Maier-Reimer, E., Kriest, I., Segschneider, J., and Wetzel, P.: The HAMburg Ocean Carbon Cycle Model HAMOCC 5.1 – Technical Description Release 1.1, Berichte zur Erdsystemforschung [Reports on Earth System Science] 14, Max-Planck-Institut für Meteorologie, Hamburg (DE), http://www.mpimet.mpg.de/fileadmin/publikationen/erdsystem_14.pdf, 2005.

Markwardt, C. B.: Non-linear Least Squares Fitting in IDL with MPFIT, in: Proceedings of Astronomical Data Analysis Software and Systems XVIII, Quebec, Canada, edited by Bohlender, D., Dowler, P., and Durand, D., vol. 411 of *ASP Conference Series*, pp. 251–254, Astronomical Society of the Pacific, San Francisco (CA), 2009.

Martin, W. R. and Sayles, F. L.: $CaCO_3$ dissolution in sediments of the Ceara Rise western equatorial Atlantic, Geochim. Cosmochim. Ac., 60, 243–263, https://doi.org/10.1016/0016-7037(95)00383-5, 1996.

Moore, J. K., Doney, S. C., and Lindsay, K.: Upper ocean ecosystem dynamics and iron cycling in a global three-dimensional model, Global Biogeochem. Cy., 18, 22, https://doi.org/10.1029/2004GB002220, 2004.

Moore, J. K., Doney, S. C., and Lindsay., K.: The Role of Ecosystem Dynamics on the Global Ocean Carbon Cycle: A JGOFS Model-Data
920   Synthesis, http://usjgofs.whoi.edu/mzweb/smpdatadocs/moore_becmodel.html, last access: 10th January 2020, 2005.

Moore, J. K., Lindsay, K., Doney, S. C., Long, M. C., and Misumi, K.: Marine Ecosystem Dynamics and Biogeochemical Cycling in the
Community Earth System Model [CESM1(BGC)] : Comparison of the 1990s with the 2090s under the RCP4.5 and RCP8.5 Scenarios, J.
Climate, 26, 9291–9312, https://doi.org/10.1175/JCLI-D-12-00566.1, 2013.

Moreira Martinez, S., Roche, D. M., Munhoven, G., and Waelbroeck, C.: Coupling MEDUSA sediment model to iLOVECLIM (v1.1β) Earth
925   system model, in: 12th International Conference on Paleoceanography (ICP12)., pp. P–368, Utrecht (NL), http://icp12.uu.nl/wp-content/
uploads/2016/08/Poster-abstracts-sessie-3.pdf, 2016.

Munhoven, G.: Modelling Glacial-Interglacial Atmospheric CO_2 Variations : The Role of Continental Weathering, Ph.D. thesis, Université
de Liège, Liège, http://hdl.handle.net/2268/161314, 1997.

Munhoven, G.: Glacial-interglacial rain ratio changes : Implications for atmospheric CO_2 and ocean-sediment interaction, Deep-Sea Res.
930   Pt. II, 54, 722–746, https://doi.org/10.1016/j.dsr2.2007.01.008, 2007.

Munhoven, G. and François, L. M.: Glacial-interglacial variability of atmospheric CO_2 due to changing continental silicate rock weathering :
A model study, J. Geophys. Res., 101, 21 423–21 437, https://doi.org/10.1029/96JD01842, 1996.

Ridgwell, A.: Interpreting transient carbonate compensation depth changes by marine sediment core modeling, Paleoceanography, 22,
PA4102, https://doi.org/10.1029/2006PA001372, 2007.

935   Ridgwell, A. and Hargreaves, J. C.: Regulation of atmospheric CO_2 by deep-sea sediments in an Earth system model, Global Biogeochem.
Cy., 21, GB2008, https://doi.org/10.1029/2006GB002764, 2007.

Seiter, K., Hensen, C., Schröter, J., and Zabel, M.: Organic carbon content in surface sediments–defining regional provinces, Deep-Sea Res.
Pt. II, 51, 2001–2026, https://doi.org/10.1016/j.dsr.2004.06.014, 2004.

Shaffer, G., Malskær Olsen, S., and Pepke Pedersen, J. O.: Presentation, calibration and validation of the low-order, DCESS Earth System
940   Model (Version 1), Geosci. Model Dev., 1, 17–51, https://doi.org/10.5194/gmd-1-17-2008, 2008.

Sigman, D. M., McCorkle, D. C., and Martin, W. R.: The calcite lysocline as a constraint on glacial/interglacial low-latitude production
changes, Global Biogeochem. Cy., 12, 409–427, https://doi.org/10.1029/98GB01184, 1998.

Soetaert, K., Middelburg, J. J., Herman, P. M. J., and Buis, K.: On the coupling of benthic and pelagic biogeochemical models, Earth Sci.
Rev., 51, 173–201, https://doi.org/10.1016/S0012-8252(00)00004-0, 2000.

945   Sundquist, E. T.: Geologic Analogs: Their Value and Limitations in Carbon Dioxide Research, in: The Changing Carbon Cycle :
A Global Analysis, edited by Trabalka, J. R. and Reichle, D. E., chap. 19, pp. 371–402, Springer-Verlag, New York (NY),
https://doi.org/10.1007/978-1-4757-1915-4_19, 1986.

Taylor, K. E.: Summarizing multiple aspects of model performance in a single diagram, J. Geophys. Res., 106, 7183–7192,
https://doi.org/10.1029/2000JD900719, 2001.

950   Tschumi, T., Joos, F., Gehlen, M., and Heinze, C.: Deep ocean ventilation, carbon isotopes, marine sedimentation and the deglacial CO_2 rise,
Clim. Past, 7, 771–800, https://doi.org/10.5194/cp-7-771-2011, 2011.

van Cappellen, P. and Wang, Y.: Cycling of Iron and Manganese in Surface Sediments : A General Theory for the Coupled Transport and
Reaction of Carbon, Oxygen, Nitrogen, Sulfur, Iron, and Manganese, Am. J. Sci., 296, 197–243, https://doi.org/10.2475/ajs.296.3.197,
1996.

955   Völker, C., Ye, Y., Butzin, M., Köhler, P., and Munhoven, G.: Role of sediment in the marine C cycle—insights from a coupled ocean-
sediment model, in: EGU General Assembly 2020, Online, https://doi.org/10.5194/egusphere-egu2020-18562, 2020.

W3C: Extensible Markup Language (XML) 1.0 (Fifth Edition), W3C recommendation 26 november 2008, W3C, http://www.w3.org/TR/2008/REC-xml-20081126, last access 2nd February 2017, 2008.

Walker, J. C. G. and Opdyke, B. C.: Influence of variable rates of neritic carbonate deposition on atmospheric carbon dioxide and pelagic
960   sediments, Paleoceanography, 10, 415–427, https://doi.org/10.1029/94PA02963, 1995.

Wenzhöfer, F., Adler, M., Kohls, O., Hensen, C., Strotmann, B., Boehme, S., and Schulz, H.: Calcite dissolution driven by benthic mineralization in the deep-sea : In situ measurements of Ca^{2+}, pH, pCO_2 and O_2, Geochim. Cosmochim. Ac., 65, 2677–2690, https://doi.org/10.1016/S0016-7037(01)00620-2, 2001.

Yool, A., Popova, E. E., and Anderson, T. R.: Medusa-1.0 : a new intermediate complexity plankton ecosystem model for the global domain,
965   Geosci. Model Dev., 4, 381–417, https://doi.org/10.5194/gmd-4-381-2011, 2001.

Zickfeld, K., MacDougall, A. H., and Matthews, H. D.: On the proportionality between global temperature change and cumulative CO_2 emissions during periods of net negative CO_2 emissions, Environ. Res. Lett., 11, 055006, https://doi.org/10.1088/1748-9326/11/5/055006, 2016.